NASA TECHNICAL NOTE

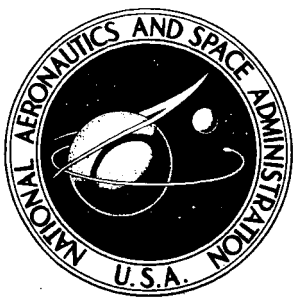

NASA TN D-7320

NASA TN D-7320

ANALYTIC AND EXPERIMENTAL PERFORMANCE OF TWO ISENTROPIC MIXED COMPRESSION AXISYMMETRIC INLETS AT MACH NUMBERS 0.8 TO 2.65

by Donald B. Smeltzer and Norman E. Sorensen

Ames Research Center
Moffett Field, Calif. 94035

NATIONAL AERONAUTICS AND SPACE ADMINISTRATION • WASHINGTON, D. C. • JUNE 1973

1. Report No.	2. Government Accession No.	3. Recipient's Catalog No.
NASA TN D-7320		

4. Title and Subtitle	5. Report Date
ANALYTIC AND EXPERIMENTAL PERFORMANCE OF TWO ISENTROPIC MIXED COMPRESSION AXISYMMETRIC INLETS AT MACH NUMBERS 0.8 TO 2.65	June 1973
	6. Performing Organization Code

7. Author(s)	8. Performing Organization Report No.
Donald B. Smeltzer and Norman E. Sorensen	A-4675
	10. Work Unit No. 764–74–01–06–00–21
9. Performing Organization Name and Address	11. Contract or Grant No.
NASA Ames Research Center Moffett Field, Calif. 94035	
	13. Type of Report and Period Covered
12. Sponsoring Agency Name and Address	Technical Note
National Aeronautics and Space Administration Washington, D. C. 20546	14. Sponsoring Agency Code

15. Supplementary Notes

16. Abstract

A mixed compression axisymmetric inlet model with a capture diameter of 50 cm was tested at Mach numbers ranging from 0.8 to 2.65 at 0° angle of attack and a constant total pressure of approximately 1 atm (a Reynolds number of $8.53 \times 10^6/m$ at Mach number 2.65). Analytical methods accounting for the effects of both viscous and inviscid flows and incorporating empirical bleed discharge coefficients were used in the procedure for designing the inlet contours and the bleed system. Experimental results are compared with analytic predictions and are also compared with results from earlier tests of an inlet with the same internal contours but with a bleed system developed by "cut and try" methods in the wind tunnel.

With the bleed configuration predicted by the design procedure, maximum total pressure recovery at the engine face at the design Mach number of 2.65 was 93 percent, with a total pressure distortion less than 10 percent. Corresponding bleed mass flow was approximately 7.5 percent, which was about 1.3 percent less than predicted. At lower supersonic Mach numbers, pressure recovery and bleed were generally lower and distortion generally higher. Performance was only slightly lower than it was for the inlet with the bleed system developed by "cut and try" methods in the wind tunnel, indicating that wind tunnel test time can potentially be reduced by using such design procedures.

17. Key Words (Suggested by Author(s))	18. Distribution Statement
Propulsion Airbreathing Inlet Internal flow	Unclassified – Unlimited

19. Security Classif. (of this report)	20. Security Classif. (of this page)	21. No. of Pages	22. Price*
Unclassified	Unclassified	57	$3.00

* For sale by the National Technical Information Service, Springfield, Virginia 22151

SYMBOLS

A	area
A_c	capture area
A_{st}	total strut area
A_x	local flow area measured normal to the inlet centerline
a	vortex generator spacing
b	vortex generator separation
d	bleed hole diameter
H	vortex generator height
h	height of boundary layer probe from surface
L	vortex generator length
l	bleed hole length
M	Mach number
ΔM	Mach number tolerance
m	mass flow
$\frac{m_{bl}}{m_\infty}$	total bleed mass-flow ratio
$\frac{m_O}{m_\infty}$	capture mass-flow ratio, $\frac{\rho_O V_O A_O}{\rho_\infty V_\infty A_c}$
N	boundary layer power law exponent, $\frac{u}{u_e} = \left(\frac{y}{\delta}\right)^{1/N}$
p	static pressure
p_p	pitot pressure
p_t	total pressure

$\overline{p}_t$ area weighted average total pressure

$p_{t_{pl}}$ plenum chamber pressure

Δp_{t_2} total pressure distortion parameter, $\dfrac{p_{t_{2\max}} - p_{t_{2\min}}}{\overline{p}_{t_2}}$

Q flow coefficient of bleed holes $\left(\dfrac{\text{actual mass flow}}{\text{theoretical sonic mass flow}}\right)$

R capture radius 24.862 cm (9.788 in.)

R′ capture radius of previous inlet model (ref. 3) 19.403 cm (7.639 in.)

r local radius

r_{cb} local radius of centerbody

r_c local radius of cowl

u velocity within the boundary layer

u_e velocity at the edge of the boundary layer

V velocity

x axial distance measured from the centerbody tip

x_c axial distance measured from the cowl lip

Δx centerbody translation from the design position (at the design position the cowl lip is at $x/R = 2.325$)

Δw stability margin to inlet unstart due to a decrease in the engine airflow demand $\left[\left(\dfrac{\overline{p}_{t_2}}{p_{t_\infty}}\right)_{\text{critical}} - \left(\dfrac{\overline{p}_{t_2}}{p_{t_\infty}}\right)_{\text{operating}} + \left(\dfrac{m_{bl}}{m_\infty}\right)_{\text{critical}} - \left(\dfrac{m_{bl}}{m_\infty}\right)_{\text{operating}}\right]$

y height within the boundary layer measured from the surface

α inlet angle of attack, deg

α_u	inlet angle of attack for incipient unstart, deg
δ	boundary-layer thickness
ρ	density

Subscripts

∞	freestream
o	inlet lip
2	engine face
bl	bleed
critical	critical conditions (i.e., just before the inlet unstarts)
exit	conditions at exit
l	local
max	maximum
min	minimum
supercritical	conditions with the terminal shock wave downstream of its critical position

NOTE: The configurations are identified in table 5.

ANALYTIC AND EXPERIMENTAL PERFORMANCE OF TWO ISENTROPIC MIXED COMPRESSION AXISYMMETRIC INLETS AT MACH NUMBERS 0.8 TO 2.65

Donald B. Smeltzer and Norman E. Sorensen

Ames Research Center

SUMMARY

The internal performance is presented for a mixed compression axisymmetric inlet model at Mach numbers ranging from 0.8 to 2.65 and 0° angle of attack. The data were recorded at a tunnel total pressure of approximately 1 atm (a Reynolds number of $8.53 \times 10^6/m$ at Mach number 2.65). The results at Mach number 2.65 are compared with inviscid predictions of the surface pressure distributions, bleed mass flow and pressure recovery, and boundary-layer profiles. In addition, a performance comparison is made between the present inlet and another inlet with the same internal contours but with a bleed pattern developed by "cut and try" methods in the wind tunnel.

The model has a capture diameter of approximately 50 cm and is 2.5 capture diameters long from the cowl lip to the engine face. Other model features are a "traveling" centerbody bleed system for off design operation, a fixed cowl bleed system, bypass and secondary air systems, cowl support struts, and vortex generators.

The supersonic diffuser was designed for near isentropic compression at Mach number 2.65 by the method of characteristics. The design provided a throat area that was 59 percent of the capture area when the centerbody was extended for transonic operation. The bleed system was designed using analytic methods that accounted for the effects of both viscous and inviscid flows, incorporated empirical bleed discharge coefficients, and included experimentally derived criteria for flow separation.

With the predicted bleed configuration and vortex generators on both cowl and centerbody, critical total-pressure recovery at Mach number 2.65 (i.e., just prior to inlet unstart) was 93.2 percent, with a total pressure distortion of 9.4 percent. The corresponding bleed mass flow was 7.3 percent, which was 1.5 percent less than predicted. At a predicted supercritical operating point, total pressure recovery was approximately 90 percent with 12 percent distortion and a corresponding bleed mass flow of 5.4 percent – 1.0 percent less bleed than predicted. Small alterations to the bleed system were required for satisfactory operation at lower supersonic Mach numbers; with these changes, total-pressure recovery and bleed were generally lower and distortion generally higher than at Mach number 2.65. A number of variations to the bleed system were tested at Mach number 2.65 but the performance was improved only slightly, indicating that the bleed design procedure was used successfully. It is concluded that valuable wind tunnel test time might be saved by employing such procedures in the design of future inlet bleed systems.

The performance at Mach number 2.65 was comparable to the performance of the inlet with the bleed system developed by "cut and try" methods in the wind tunnel. At lower supersonic

Mach numbers the performance was better for the inlet with the "cut and try" bleed system, but this inlet required removal of the vortex generators for satisfactory performance at these conditions.

INTRODUCTION

Until recently the bleed systems necessary for high performance supersonic inlet systems were developed in wind tunnels by "cut and try" methods. These methods are time consuming and expensive in terms of wind tunnel testing costs. Now with a recently developed design procedure (refs. 1 and 2), bleed systems can, in principle, be designed so that only fine tuning of the bleed system will be required in the wind tunnel. The primary purpose of the present investigation was to determine experimentally the validity of the design procedure. A secondary goal was to compare the performance with the performance of an inlet system which had a bleed system developed by "cut and try" methods in the wind tunnel (ref. 3).

The internal contours were designed for Mach number 2.65. The design procedure for the bleed system was applied over the Mach number range 1.8 to 2.65. The procedure accounted for both the viscous and inviscid flows, used experimental criteria for flow separation, and used experimental results for the flow coefficients of bleed holes. These analyses were used to predict a configuration for the bleed system. Vortex generators were also included downstream of the throat to reduce the flow distortion at the engine face.

Experimental results were obtained from a large scale model in the Ames Unitary Plan Wind Tunnels at Mach numbers 0.8 to 2.65 and a constant total pressure of about 1 atm (a Reynolds number of $8.53 \times 10^6/m$ at Mach number 2.65). [The same facilities and test conditions were used for the inlet with the "cut and try" bleed systems (ref. 3).] A photograph of the model mounted in one of the wind tunnels is shown in figure 1.

Total-pressure recovery and distortion at the engine face were measured as a function of bleed mass flow. In addition, surface pressure distributions, boundary-layer profiles, and inlet sensitivity to unstart caused by changes in angle of attack or Mach number were measured. Results were obtained for different bleed and vortex generator configurations.

MODEL

A sketch of the model is shown in figure 2 and the coordinates of the internal contours are presented in table 1. The capture diameter was 49.724 cm (19.576 in.). The model had a remotely controlled centerbody that translated from $\Delta x/R = -0.015$ to $\Delta x/R = 1.555$ (transonic position). Both the cowl and centerbody bleed systems were divided into isolated plenums. From these plenums the flow was discharged overboard through calibrated exits, the areas of which could be varied manually on the model. Four struts supported the cowl and provided ducting to the centerbody bleed exit plenums located on the cowl. The bypass and secondary air systems were located just upstream of the engine face. Air passed through the bypass gap into a plenum and was discharged to the freestream through the bypass doors and/or secondary airvalves. Both the bypass doors and secondary air valves were remotely controlled. At the engine face, total pressures were

measured with rotating rakes; downstream of the engine face there was a mass flow control plug (not shown) to vary the position of the terminal shock wave. Rotation of the rake and translation of the plug were remotely controlled.

Details of the bleed system and the initial location for the vortex generators are shown in figure 3. Tables 2 and 3 show the location of all of the bleed holes available on the model. The bleed hole sizes, locations, and angles were obtained from the design procedure to be discussed later. The cowl bleed flow was discharged into three isolated plenums. Each plenum was divided circumferentially at 90° increments to minimize possible cross flow. The bleed holes for plenums 1, 2 and 3 were drilled at 20°, 40°, and 90° from the wall, respectively.

The centerbody bleed system was considerably more complex since the design features of this inlet required a unique boundary layer bleed system for the translating centerbody. For good performance, boundary-layer removal from the centerbody surface near the inlet "throat" (minimum flow area) was required for supersonic Mach numbers greater than 1.6. With this inlet design, the location of the inlet throat remained fixed relative to the cowl as the centerbody was extended from the $M = 2.65$ design position. Consequently, the location of the inlet throat relative to the centerbody and the regions on the centerbody from which boundary layer had to be removed changed as the centerbody was extended. To accomplish the changes in location of the required bleed regions, a unique "traveling" boundary layer bleed system was devised (ref. 2). The elements of the system were seventeen compartments and two ducts within the centerbody support tube through which bleed air could be directed to the exits. The seventeen compartments within the centerbody (fig. 3) were arranged such that each provided a connection between the boundary layer removal holes on the surface of the centerbody and the two ducts within the support tube through a valving arrangement (much like a conventional sleeve valve). Proper arrangement of the receiving slots in the centerbody support tube and the discharge slots from the centerbody compartments provided the desired changes in location of boundary-layer removal from the centerbody surface as the centerbody was extended. Figure 3 shows the compartments (starred superscript) that were "active" and "bleeding" at the design position ($\Delta x/R = 0$). Plenums 1 and 2 discharged into the forward bleed duct and 4 and 5 into the throat bleed duct. The flow into all other compartments was blocked from the ducts by the support tube surface. From the support tube bleed ducts, the flow passed through separate passages in the support struts into isolated exit plenums and was discharged overboard through louvers. By extending the centerbody, plenums were opened and closed according to a predetermined bleed "schedule."

The predicted bleed schedule for the centerbody is shown in figure 4 (configuration 1). Also shown are predicted centerbody positions for operation at some of the off-design supersonic Mach numbers. These predictions were a necessary part of the bleed system design, as will be discussed later. The cross hatched columns indicate plenums discharging to the forward bleed duct and the solid columns those discharging to the throat bleed duct. For instance, if the centerbody was extended to $\Delta x/R = 0.15$, plenums 2 and 3 would discharge to the forward bleed duct and plenums 5, 6, and 7 to the throat bleed duct. Early in the test it was found that with the predicted bleed schedule, there was terminal shock wave instability when the centerbody was translated through the "gaps" in the forward bleed (e.g., $\Delta x/R = 0.23$ to 0.30 for plenum 3). Therefore, the bleed schedule was changed to the modified schedule (configuration 2). This change was accomplished by varying the items labelled "inserts" in figure 3. Note that although this change eliminated the "gaps," it did not change the bleed at the Mach number 2.65 design position, $\Delta x/R = 0$. The active bleed holes for the predicted centerbody positions at Mach numbers 2.65 and 2.50 and for

this revised schedule are shown in figure 5. Note that the skin thickness is constant for both cowl and centerbody. This means that the length to diameter ratio for the 20° and 40° holes is greater than for the 90° holes. This factor influences the flow coefficient of the holes and will be discussed later.

INSTRUMENTATION

Detailed instrumentation consisting of static and total pressure rakes and static pressure orifices was used to measure the internal performance. Total-pressure recovery and distortion at the engine face were calculated with pressure measurements from eight equally spaced rakes, each with seven tubes spaced on an area weighted basis. Bleed mass flows were calculated from pressure measurements in the bleed plenum and pre-test calibrations of the bleed exits. Surface pressure distributions were measured with static pressure orifices located on the inner surface of the cowl and centerbody. Pitot-pressure profiles in the boundary layer were measured with rakes at several locations on the cowl and centerbody. Transonically ($M_\infty = 0.8$ to 1.4), the inlet capture mass flow was calculated with pressure measurements from a single rake located at the throat. This rake measured both static and total pressures. Pressure measurements also were made in the bypass plenum, in the secondary air duct, on the external surface, and near the mass flow plug (for mass flow at the engine face). Results from these measurements are not included in this report.

DESIGN

The supersonic diffuser, subsonic diffuser, cowl support struts, and many features of the bypass system were the same as for the inlet system reported in reference 3. The design of these components was discussed in detail in that reference and they are therefore mentioned only briefly in this report. Conversely, since the bleed system and vortex generators used for the two inlets were considerably different, and since the secondary air system was used only in the present inlet, the design of these components is discussed in more detail.

Supersonic Diffuser

The supersonic diffuser contours were designed with the aid of the method of characteristics (ref. 4). The major goals were to design contours which compressed the flow nearly isentropically to a Mach number of 1.25 in the throat at the design Mach number of 2.65 and to accomplish this task with contours that provided nearly the maximum possible throat area ($0.595A_c$) when the centerbody was extended for transonic operation. (Other design concepts (ref. 5) can provide a greater transonic throat area but a translating centerbody has the least mechanical complexity.) The data in reference 3 show that these goals were closely met.

Subsonic Diffuser

The subsonic diffuser contours were designed to avoid losses due to flow separation with an area distribution that had a reasonably uniform growth rate downstream of the throat during

transonic operation. In fact, this transonic area requirement determined the contour of the centerbody downstream of $x/R = 4.25$.

Cowl Support Struts

The cowl support struts were sized for the expected centerbody boundary-layer bleed flow. Four struts were used in the present case, whereas three were used on the model described in reference 3; the total strut area was approximately the same for both models. The contours of the struts, the subsonic diffuser, and the supersonic diffuser gave the area distributions shown in figure 6. The total strut area distribution is shown separately.

Bypass and Secondary Air System

The bypass and secondary air systems received flow from a common gap just upstream of the engine face (fig. 2). The bypass doors were part of the smooth external contour when closed. The secondary air passage was sized to pass approximately 6 percent of the capture flow at Mach number 2.65. This flow was controlled with the secondary air valves (fig. 2). The round lip on the downstream edge of the gap helped to minimize the losses of the bypass and/or secondary airflow passing through the gap from the main duct.

Vortex Generators

Triangular vortex generators were used for the present model whereas the generators were rectangular for the model in reference 1. Table 4 shows the geometric dimensions of the vortex generator configurations used for this test as well as the configuration used for the model described in reference 3. The rectangular generators were 12 percent thick airfoils while the triangular generators were 0.16 cm thick plates with rounded leading edges and blunt trailing edges.

It is important to note that as the centerbody was extended for off-design operation, the vortex generators on the centerbody entered the supersonic flow field; rather severe performance penalties resulted when rectangular generators were in supersonic flow (ref. 3). However, unpublished results indicated that these penalties would be less for triangular than for rectangular generators and that fewer pairs of generators would probably be sufficient to reduce the total pressure distortion at the engine face to an acceptable level. Consequently, a relatively sparse distribution of triangular generators was used for the present inlet.

Bleed System

The bleed system was designed using the procedure described in references 1 and 2. Briefly, the methods are as follows. The centerbody position for an inviscid throat Mach number of 1.25 was computed over the Mach number range for started inlet operation (M_∞ = 2.65 to 1.6) using a computer program employing the method of characteristics. Next, the boundary layer on both cowl and centerbody was calculated using a finite difference solution of the boundary-layer equations (ref. 1). From the boundary-layer calculations, contour maps of the boundary-layer power law

exponent N were made as shown in figure 7. Shock wave impingement locations and lines of constant centerbody boundary-layer power law exponent are plotted as a function of centerbody station for the full range of started Mach number centerbody positions. (Note that there is no computer solution downstream of the second shock because the solution indicates detachment (i.e., subsonic flow without bleed).) Experimental results from similar inlets have shown that separation is imminent when N is approximately 3 or less in the supersonic diffuser upstream of the throat or less than 7 in the region of the throat. It should be noted that when mass is removed through a bleed area, the velocity distribution through the boundary layer at the beginning of the bleed area is changed from its predicted distribution – one that is near separation – to a more fully turbulent profile at the end of the bleed area. The profile established, of course, depends on the amount of mass removed through the bleed area. That is, immediately upstream of the bleed region, the boundary-layer equations are solved subject to the wall boundary conditions where the velocity on the wall is zero and there is no flow through the wall. In the bleed region, the second condition is not zero and the boundary-layer equations are solved continuously based on the amount of mass removed. Downstream of the bleed region the original boundary conditions are again imposed. Thus, various values of the bleed mass flow ratio are tried in the bleed area until just enough of the boundary layer is removed to prevent separation. This procedure is used for each bleed region until the minimum total mass removal is found to eliminate separation everywhere along the surfaces.

The bleed hole slant angles were determined using experimental results for the performance of bleed holes as reported in reference 6. An example of bleed hole performance is shown in figure 8 where the flow coefficient of holes Q is plotted as a function of the bleed flow total-pressure recovery. Data are shown for two local inviscid flow Mach numbers and three hole slant angles θ. Three important flow characteristics are evident from the curves: (1) the flow coefficient Q increases with decreasing slant angle θ; (2) the pressure recovery is higher (i.e., bleed drag is lower) for a given Q as θ decreases; and (3) the ratio of Q at lower Mach number to Q at a higher Mach number (i.e., the change in bleed with change in Mach number) increases with increasing θ. Characteristic 3 was important because the throat bleed system was designed for a relatively large change in bleed as the terminal shock wave moved in the throat, thus contributing to the stability margin Δw, as will be discussed later; therefore, 90° holes were used in the throat. In the mid bleed regions, 40° holes were used as a compromise between characteristics 2 and 3, since some contribution to Δw had been observed for the model of reference 3. In the forward regions, 20° holes were used so that the bleed pressure recovery would be as high as possible.

The size of the bleed holes relative to the boundary-layer height was also considered. Unpublished results showed that holes with a diameter approximately equal to the boundary-layer displacement thickness offered minimum disturbance to the inviscid portion of the flow. However, it was anticipated that some alterations to the bleed pattern would be required in the wind tunnel (the bleed pattern was altered by opening holes or filling them with dental plaster). Holes of 0.159 cm diameter, approximately twice the displacement thickness, were chosen to facilitate the alterations.

The last parts of the bleed system to be designed were the exits. The mathematical analysis is described in reference 7. Convergent-divergent nozzles were used for the throat bleed exits and convergent nozzles for the forward bleed exits. The nozzle exit areas were sized so that the system operated near the "knee" of the curves in figure 8, thus giving reasonably high plenum pressures (i.e., low bleed drag) and large flow coefficients for the bleed holes.

The predicted performance of the bleed system at Mach number 2.65 is shown in figure 9. The curves of bleed mass flow versus plenum pressure recovery were calculated from inviscid pressure distributions and Mach numbers, duct total pressures, the bleed hole areas, and experimentally determined flow coefficients for similar bleed holes (fig. 8). For the throat bleed, several curves are shown because the local inviscid flow Mach numbers and surface pressures changed as the terminal shock wave moved in the throat. Also shown is the line of mass flow versus plenum pressure for the fixed exit areas. The predicted bleed mass flow and plenum pressure recovery is at the intersection of these two sets of curves. Predicted bleed system performance at two inlet conditions is shown: (1) at critical conditions just before the inlet unstarts; and (2) at the operating condition where there is a resistance to inlet unstart caused by a decrease in the engine airflow demand ($\Delta w = 0.05$).

For the forward bleeds, predicted performance does not vary because the terminal shock wave was not expected to influence pressures in these regions. For the mid bleed on the cowl, the terminal shock wave was expected to feed forward through the boundary layer at critical conditions; hence, a slight increase in bleed was predicted. For the throat bleeds, the surface Mach number was expected to vary between about 0.75 and 1.25, so that a larger change in bleed was predicted. The increase in total bleed from operating to critical conditions was predicted as 0.023. Thus, the remainder of the resistance to inlet unstart at the operating point will result from an increase in total pressure recovery at the engine face as the terminal shock wave moves upstream.

MEASUREMENT TECHNIQUES AND ACCURACY

The following table shows the estimated accuracy of the primary parameters:

Parameter	Accuracy
p_t/p_{t_∞}	±0.010
$\bar{p}_t/p_{t_\infty}$	±0.002
Δp_{t_2}	±0.02
m_{bl}/m_∞	±0.003
α	±0.10°
p/p_∞	±0.2
M_∞	±0.005
m_2/m_∞	±0.010 (transonic test only)

The measurement techniques and accuracies of all parameters except mass-flow ratio have been established from many similar tests at the Ames Unitary Plan Wind Tunnels. The accuracy of the bleed mass flow ratio was established from bench calibrations where the mass flow was measured as a function of the bleed exit plenum pressure for the spectrum of pressures encountered in the wind tunnel.

At transonic Mach numbers, the capture mass flow was calculated from static and total pressure measurements at the throat. This method was used successfully for the inlet model reported in reference 3. The earlier model had four rakes mounted 90° apart whereas one rake was used for the present model. This modification was deemed sufficient, based on results from the earlier tests.

RESULTS AND DISCUSSION

The principal performance parameters considered in this investigation are total-pressure recovery and total-pressure distortion at the engine face as a function of bleed mass flow at supersonic Mach numbers, and as a function of mass flow at the engine face at transonic Mach numbers. At supersonic Mach numbers, mass flow at the engine face with the inlet started is the difference between the capture mass flow and the bleed mass flows; inlet capture mass flow is shown in figure 10 as a function of centerbody position. The discussion is presented in three subsections: (1) the comparison of experimental results with analytic predictions; (2) the effect of alteration of the bleed and vortex generator configuration on performance; and (3) a comparison of performance between the present inlet and the previous inlet reported in reference 3. All of the results are for 0° angle of attack.

The data in this report are only a small sampling of that obtained during testing. Additional data not included in this report are included in reference 2. A listing of the model configuration parameters is shown in table 5.

Analytical and Experimental Performance with the Predicted Bleed Configuration

The feasibility of designing a supersonic diffuser using only inviscid calculations and allowing the bleed system to compensate for the displacement thickness of the boundary layer can be judged by comparing the experimental centerbody positions where the inlet chokes and unstarts with the calculated positions for an inviscid choked throat. These comparisons are shown in figure 11 at Mach numbers 2.5 and 2.6. The experimental position was measured with the terminal shock wave well downstream of the throat; hence it did not influence the experimental results. The agreement is good for configuration 1 at Mach number 2.60. However, at Mach number 2.50, the inlet unstarted at $\Delta x/R = 0.273$; at this centerbody position, there is a "gap," as described in Bleed System Design, in the centerbody plenum 3 bleed (see fig. 4). When the schedule was altered to eliminate the "gaps" (configuration 2), the choked centerbody position was much closer to the calculated position of $\Delta x/R = 0.233$. As a result, this altered schedule was used for the remainder of the test.

These experimental results (fig. 11) also show centerbody positions where the freestream Mach number could be decreased by 0.05 without requiring control action to prevent inlet unstart. That is, the inlet will remain started in the region above the line in figure 11; therefore, if the inlet is operated at Mach number 2.65 with the centerbody position for inlet unstart at Mach number 2.60, the Mach number can decrease by 0.05 without unstarting the inlet. This Mach number decrease is called the Mach number tolerance. A tolerance of 0.05 was considered sufficient to avoid inlet unstart for almost all sudden Mach number changes in flight caused by disturbance such as gusts. (In

the wind tunnel the Mach number could only be changed slowly, whereas in flight, it changes rapidly.) Therefore, most results in this investigation were recorded at centerbody positions (contraction ratios) where the Mach number tolerance was 0.05.

The principal performance parameters of total-pressure recovery and total-pressure distortion at the engine face as a function of bleed mass flow are plotted in figure 12 for configuration 2 at Mach numbers 2.65 and 2.50. Critical pressure recovery is approximately 93 percent for both Mach numbers and the distortion is approximately 10 percent. However, inlets are not normally operated at critical conditions because some stability margin, Δw, is required to prevent the inlet from unstarting due to sudden decreases in engine airflow demand that cannot be accommodated soon enough by action of the inlet control system (e.g., extending the centerbody and/or opening the bypass doors). If the inlet is operated with the terminal shock wave downstream of its critical position, there is a stability margin because the increase in bleed and pressure recovery that occur as the terminal shock wave moves upstream compensates for a decrease in engine airflow demand. An operating condition where the stability margin is 0.05 is shown in the figure. Distortion is relatively high at this condition while bleed mass flow is considered to be low to moderate for the indicated pressure recovery.

Another important parameter, the inlet angle of attack for incipient unstart (α_u), is shown for Mach number 2.65 (fig. 12). This parameter indicates the angle of attack range from 0° over which the inlet will remain started without inlet control action (fixed geometry). This range increases from no tolerance at critical pressure recovery to a limiting value of 2.0° at a pressure recovery of 89 percent or lower. The α_u range at $\Delta w = 0.05$ will be less than 2°, which is considered to be a minimum requirement for most transport missions. The asymmetry between positive and negative angles could be due to a slight stream angle in the wind tunnel, asymmetric bleed or model geometry, or a combination of all of these items.

The bleed mass flow through each isolated plenum or duct is shown in figure 13 for the configuration just discussed. The data show the bleed regions that contribute to the inlet stability margin: At Mach number 2.65 only the throat bleeds change as the terminal shock wave moves upstream, while at Mach number 2.50, there is at least a small change in bleed in cowl plenum 2.

Experimental bleed rates are compared with the analytic predictions in figure 14. (The predictions are repeated from figure 9.) Experimental results are shown at critical conditions and with a stability margin Δw of 0.05. Note that the experimental bleed rates for a stability margin of 0.05 are not actual data points but are interpolations from the previous figure. The experimental bleed rates and plenum pressures are less than predicted for the forward bleed regions on both cowl and centerbody. The experimental bleed rates and plenum pressures were quite close to predictions for the mid bleed region on the cowl. However, there was no change in this bleed from the operating to the critical condition, as was expected from the tests of reference 3. The experimental bleed rates and plenum pressures in the throat were close to predictions for the centerbody and somewhat low for the cowl. However, the change in experimental bleed from operating to critical conditions was in good agreement with predictions for both the cowl and centerbody. Overall, the measured change in total bleed mass flow from the operating to the critical point was 0.019, only 0.004 less than the predicted value of 0.023.

As previously mentioned, predictions of bleed rates were based on local total pressures. Since predicted and experimental local total pressures were in good agreement for the previous inlet

(ref. 3), they were assumed to be in good agreement for the present inlet and hence, not a cause of differences in predicted and experimental bleed rates. The difference between predicted and experimental surface static pressure distributions, however, can be used to explain the differences between predicted and experimental bleed rates since they are an indication of the surface Mach number which is used to select the proper flow coefficient for the bleed holes. These pressures are compared at Mach number 2.65 in figure 15. Experimental results are shown at critical conditions and for the operating condition (data point on fig. 12 nearest $\Delta w = 0.05$). The predictions are for supersonic flow only and do not allow for the pressure rise through the terminal shock wave. Also shown are sketches of the inlet contours, the predicted internal shock structure, and the bleed system. Pressures at the forward bleeds on both surfaces are in good agreement with theory; therefore, the flow coefficient used for these bleed predictions should be correct. Pressures at the mid cowl bleed are lower than predicted at the operating condition. The Mach number is, therefore, higher than predicted and the flow coefficient used for this bleed prediction is too high. In the throat, selection of the proper flow coefficient requires accurate estimation for the location of the terminal shock wave. It was expected to be at $x/R \simeq 4.25$ to 4.30 for the operating condition and at $x/R \simeq 4.1$ to 4.15 for the critical condition, based on results from the previous inlet (ref. 3). For the prediction of bleed rates, the pressure rise through the terminal shock wave was assumed to be sudden and sharp as opposed to the more gradual rise seen experimentally. (Experimentally, the terminal shock wave is assumed to be located in the region of large pressure rise from supersonic to subsonic flow (e.g., $x/R = 4.17$ to 4.26 at critical conditions on the cowl).) Thus, it is less likely that the proper flow coefficient was selected for the throat bleed than it was for the forward bleed calculations.

The ratio of bleed hole length to diameter is another factor that can also affect the flow coefficient of the bleed holes and hence, the calculation of bleed rates (ref. 6). Flow coefficients for all bleed predictions were based on a ratio of 3, while the actual ratio was 5 for the number 1 plenum on both surfaces. Hence, the experimental flow coefficient was less than expected.

The pressure distributions in figure 15 show that the pressure rise through the terminal shock wave at critical conditions is "sharper" on the cowl than on the centerbody. That is, on the cowl the pressure rise occurs from $x/R = 4.17$ to 4.26, while on the centerbody it occurs from $x/R \simeq 4.05$ to 4.25 or twice the distance. The sharper rise on the cowl indicates better control of the boundary layer on this surface. Bleed at the foot of the terminal shock wave at $x/R \simeq 4.05$ to 4.10 on the centerbody might have provided better control of the centerbody boundary layer at critical conditions. At the operating point, there is bleed at the "foot" of the terminal shock wave, $x/R = 4.2$, and the pressure rise occurs over approximately the same distance on both surfaces.

Experimental Performance With Different Bleed and Vortex Generator Configurations

Different bleed and vortex generator configurations were tested in an effort to improve the overall performance. A summary of the performance at Mach number 2.65 for different bleed configurations is shown in figure 16. The differences in these configurations are shown in table 5. Total pressure recovery and distortion at the engine face and the corresponding bleed mass flow is shown at critical conditions and with a stability margin Δw of 0.05. The centerbody position where the inlet unstarts at Mach number 2.60 is also shown. These positions are significant because if the inlet is operated at these positions or at greater positive values of $\Delta x/R$ at Mach number 2.65, the Mach number tolerance is at least 0.05. The different configurations resulted in

only small differences in performance, although with configuration 7, the inlet had a Mach number tolerance greater than 0.05 at the design centerbody position of $\Delta x/R = 0$. For this reason, the bleed pattern for configuration 7 was used for all later configurations. Configuration 9 was the same as 7 except that the exit area for cowl plenum 1 was reduced. Since this reduced area increased the operating plenum pressure recovery, it was used for configurations 10 through 18.

Various vortex generator configurations were investigated for the bleed pattern of configuration 7 (see table 4). These results are shown in figure 17(a) for Mach number 2.65. Note that the bleed exit areas are not the same for all configurations (table 5), although for each of the three pairs of configurations shown, the areas are equal. The performance at the engine face with small and large cowl vortex generators (configurations 9 and 10) shows that at and near critical conditions, small cowl generators are better since total-pressure recovery is higher for the same bleed mass flow. At a stability margin of 0.05, however, the performance is nearly the same because the trade of bleed versus pressure recovery is about equal. The performance with centerbody vortex generators located forward and aft (configurations 11 and 13) shows that the aft location is slightly better at a stability margin of 0.05 because bleed is about the same while pressure recovery is slightly higher. For the two comparisons just discussed, distortion is near 10 percent or less for a stability margin of 0.05 or less. The performance with and without cowl vortex generators (configurations 18 and 13) shows that at and near critical conditions, pressure recovery and distortion are higher at a fixed bleed mass flow without cowl generators. However, when operated with a stability margin of 0.05, cowl vortex generators significantly increase pressure recovery and lower distortion. Overall, the performance is highest with aft located centerbody vortex generators and small cowl vortex generators (configuration 9). However, the configuration used for testing at lower Mach numbers was configuration 18, which did not have cowl generators because previous experience indicated that they were detrimental to the transonic performance (ref. 3). At Mach number 2.50 (fig. 17(b)), the best vortex generator configuration was the same as that tested at Mach number 2.65 (configuration 9). However, the performance without cowl vortex generators was slightly better at Mach number 2.50 than at Mach number 2.65.

It was previously mentioned that at any given centerbody position there were many open but inactive centerbody bleed holes. It was not expected that inactive holes in the subsonic diffuser would cause performance penalties, although this assumption was not verified experimentally. However, inactive holes in the supersonic diffuser were expected to reduce the performance because of surface roughness. This expectation is verified for Mach number 2.65 in figure 18, where the performance at the engine face is shown with the holes in centerbody plenum 3 alternately open and closed. At critical conditions, pressure recovery was about the same and the corresponding bleed mass flow was slightly higher with the inactive holes open. With a stability margin of 0.05, pressure recovery was again about the same for both configurations; however, bleed mass flow was higher with the inactive holes open. (The small difference in centerbody position for the two configurations was thought not to have caused the difference in performance.) Unfortunately, these holes were needed for boundary-layer removal at lower Mach numbers and thus had to be open. It is possible that the trade of pressure recovery for bleed would have been favorable if the inactive holes had bled at Mach number 2.65; however, this was not possible because of model limitations.

Performance Comparison With a Previous Inlet Model (Ref. 3)

The "cut and try" bleed hole configuration of the previous inlet and the predicted configuration of the present inlet are shown in figure 19. The bleed configurations are shown for Mach

number 2.65 and the design centerbody position of $\Delta x/R = 0$; it should be noted that the supercritical bleed rates at Mach number 2.65, with the terminal shock wave well downstream of the throat, were nearly the same on each surface for the two systems. The previous inlet had two isolated bleed plenums on the cowl, whereas the present model has three. On the centerbody, each model had two isolated bleed plenums. In addition, the bleed holes of the previous model were twice the diameter of the holes in the present inlet model. Moreover, all holes on the previous model were drilled normal to the surface and the length to diameter ratio (l/d) was the same for all holes.

Another important difference between the two models was in the "schedule" of bleed with centerbody translation. The schedules for the two inlets are compared in figure 20. The Mach numbers and corresponding centerbody positions where data were obtained are also indicated. At the centerbody position indicated for each Mach number in the present model, the Mach number tolerance was not measured; the indicated bleed locations and centerbody positions gave the best performance. Note that for the previous model, all bleed was considerably upstream of the throat at some Mach numbers, while on the present model, there was always bleed downstream of the throat. In addition, the centerbody positions at lower Mach numbers were, different in some cases. Another important difference was that all bleed holes were always open for the present inlet while the inactive holes were filled with dental plaster and sanded smooth for the previous inlet. Therefore, the effect of open but inactive holes on performance is not known for the previous inlet.

The vortex generators were also different for the two models. The configurations that gave the best performance at Mach number 2.65 are shown in table 4 (indicated as initial configuration for the present model). The generators differed in size, shape, and spacing but the axial location on the cowl and centerbody were about the same. Note that the dimensions are expressed as ratios to the capture radii, which were different for the two models (see symbols).

A comparison of the supercritical performance for the two inlets at Mach number 2.65 is shown in figure 21. Both models have about the same Mach number and angle of attack tolerance as well as nearly the same supercritical bleed flow with the terminal shock wave well downstream. Pressure recovery and bleed mass flow are higher for the previous model at critical conditions because, as will be seen later, the terminal shock wave is further upstream and the bleed increases in the forward bleed regions. At $\Delta w = 0.05$, pressure recovery is higher for the previous model but at the expense of higher bleed flow. At both conditions, the trade of bleed versus pressure recovery is considered only slightly favorable for the previous inlet model. Perhaps the greatest difference is in the distortion, which is lower for the previous model over a larger operating range.

If the performance comparison is made in terms of bleed versus pressure recovery, the present inlet is better over the bleed mass flow range 0.055 ot 0.065. However, the inlet has a lower stability margin over this range because the change in both bleed and pressure recovery is less as the terminal shock wave moves upstream toward critical conditions. For instance, at a bleed mass flow of 0.056, the pressure recoveries and stability margins are 0.911 and 0.038 versus 0.907 and 0.058 for the present and previous models, respectively. Most of the relatively small change in bleed for the present model, from $m_{bl}/m_{\infty} = 0.056$ to critical conditions, is caused by a relatively small change in centerbody bleed. This observation is verified by the comparison of the supercritical bleed flows through the individual plenums shown in figure 22. Note that changes in bleed in all plenums contributed to the stability margin for the previous inlet while only the throat bleed changed for

the present inlet. Nevertheless, the total change in cowl bleed from the supercritical operating condition (total bleed = 0.056) to critical conditions, is comparable for the two inlets (0.011 and 0.012). The total change in centerbody bleed, however, is considerably greater for the previous inlet (0.012 versus 0.0045). The expected trend in the centerbody throat bleed for the present inlet is indicated by the dashed line. If the centerbody bleed had followed this line, the bleed at pressure recoveries of 90 to 91 percent would have been near the minimum supercritical value of 0.008. This process, in turn, would have increased the change in centerbody throat bleed from operating to critical conditions and hence, would have increased the stability margin. Put in other terms, the total bleed at a stability margin of 0.05 might have been less with no decrease in pressure recovery.

The centerbody throat bleed did not follow this expected trend because at a pressure recovery of 90 to 91 percent, the terminal shock wave was further upstream than expected. This result is shown by the comparison of centerbody static pressure distributions in figure 23(a). A sketch of the contours and bleed systems of the two inlets is also shown. At a pressure recovery of 90 to 91 percent for the present inlet, the terminal shock wave is located between the pair of rows of throat bleed holes ($x/R \simeq 4.25$), whereas it was expected to be nearer $x/R = 4.30$. However, pressure recovery is only about 88 percent when the terminal shock wave is near this latter location. If the throat bleed had been concentrated near $x/R = 4.2$, as it was for the previous inlet, a change in throat bleed might have been delayed to a higher pressure recovery. Another factor influencing the change in centerbody bleed is the location of the terminal shock wave at critical conditions. At this condition, the terminal shock wave influences pressures considerably upstream of its actual location. For the previous inlet, the pressures changed over the open forward centerbody bleed holes ($x/R \simeq 4.1$) and naturally this bleed increased at critical conditions. On the present model, there were no bleed holes open at $x/R \approx 4.1$; active bleed holes might have increased the critical bleed flow.

Similar comparisons of surface pressure distributions on the cowl are shown in figure 23(b). At critical conditions the terminal shock wave boundary-layer interaction increases the pressure upstream of the terminal shock but not to the extent that it did on the centerbody. This observation indicates that the boundary layer is thinner on the cowl than on the centerbody. This situation might be expected since the forward cowl bleed mass flow is greater than the forward centerbody bleed mass flow for both models. For the previous inlet, the pressures increase over some of the forward bleed holes as the terminal shock wave nears its critical location and therefore, the forward bleed increases. For the present inlet pressures in this region did not increase and as a result, the forward and mid-cowl bleeds were constant for all positions of the terminal shock wave.

The relatively low pressure recovery at and near critical conditions for the present inlet (see fig. 21), is attributable to relatively low recovery near the centerbody. This is shown by the radial total-pressure profiles at the engine face in figure 24. The average of pressures measured at a fixed radius are shown for a supercritical point where the bleed mass flow is the same for the two inlets ($m_{bl}/m_{\infty} = 0.056$), and for the critical points (m_{bl}/m_{∞} unequal). Also shown is a curve of the incremental pressure recovery for each inlet between these two operating conditions. For the previous inlet, pressure recovery increases radially across the entire duct from supercritical to critical conditions. For the present inlet, however, pressure recovery is nearly constant near the centerbody for the two conditions shown. In fact, at $r/R = 0.545$, the pressure recovery at critical conditions is less than at supercritical conditions (the increment is negative), and the boundary layer near the centerbody may be on the verge of separation since the total pressure at $r/R = 0.43$ is only slightly higher than the surface static pressure.

Calculation of boundary-layer profiles was a necessary part of the analytic methods used to design the bleed system. Predicted profiles of boundary-layer pitot pressure on the cowl are compared with experimental results in figure 25. Note that the predictions are only for the present inlet; predictions would be different for the previous inlet (ref. 3) because the bleed system is different. In addition, the experimental results for the present inlet are for configuration 18, but the difference in bleed hole location between these configurations is small (see table 5). The theoretical and experimental boundary layer heights are in good agreement upstream of all bleed regions ($x/R = 3.60$). However, experimentally measured pressures are lower than predicted. At $x/R \simeq 3.95$, the boundary layer is slightly thicker and the pressures in the boundary layer are lower for the previous than for the present inlet. Note that the station for these measurements was in a region of bleed holes in cowl plenum 1 for the previous inlet and downstream of the bleed holes of cowl plenum 1 for the present inlet (see figure 19). At $x/R \simeq 4.15$, the profiles for the two inlets are similar. However, the boundary layer is thicker than predicted. Note that this station is between cowl plenums 2 and 3 for the present inlet but is near the aft edge of cowl plenum 1 for the previous inlet. These results are typical and clearly indicate a need to improve the methods to predict the boundary-layer characteristics in such inlet systems.

Most of the previous discussion compared results at the design Mach number of 2.65. Comparisons at off-design Mach numbers are also needed to complete the evaluation of inlet performance. A comparison of the performance of the two inlet systems at off-design supersonic Mach numbers is shown in figure 26 for the bleed schedules shown in figure 20. Total-pressure recovery and distortion at the engine face, the corresponding bleed mass flow, and the centerbody position are shown at critical conditions and with a stability margin of 0.05. Note that the data for the present inlet are for configuration 18 (vortex generators only on the centerbody). This was not the best configuration based on the performance at Mach number 2.65 (see fig. 17), but was used for reasons previously discussed. In addition, results without vortex generators are shown for the previous inlet because the generators caused rather severe performance penalties at off-design Mach numbers. Pressure recovery is higher both at critical conditions and at the operating point for the previous inlet, while bleed is about the same or slightly higher. Distortion is about the same for both inlets at the operating point while at critical conditions, it is lower for the previous inlet. At the operating point, distortion is relatively high for both inlets. Overall, the performance at off-design supersonic Mach numbers is better for the previous than for the present inlet. However, the off-design supersonic performance of the present inlet would probably have been better with vortex generators on both cowl and centerbody, while the performance of the previous inlet would probably have been lower with a traveling bleed system that had "open but inactive" holes in the supersonic diffuser. This observation means that for two operational systems, the differences in performance would not be as great as shown. Moreover, at Mach numbers 1.6 to 1.8, the bleed mass flow of the present inlet is only 0.01. This result was at least partially due to a recirculation of the centerbody bleed flow, as discussed in reference 2. The performance would probably have been considerably better had the recirculation not been present and had the bleed rates been higher.

A comparison of the performance of the two inlets at Mach numbers 0.8 to 1.4 is shown in figure 27. Total-pressure recovery and distortion at the engine face are shown as a function of mass flow at the engine face. Also shown is the bleed mass flow for the present inlet. Note that the bleed exits were closed for the previous inlet so that all the capture mass flow would be available at the engine face. Also, the vortex generator configurations were the same as at off-design supersonic Mach numbers. At the only common Mach number, $M_\infty = 0.8$, maximum mass flow at the engine face was higher for the previous than for the present inlet. This result was expected because the

bleed exits were closed for the previous inlet. However, an inlet will not normally oeprate at maximum mass flow because of relatively low pressure recovery and high distortion. If operated at reduced mass flow, say $m_2/m_\infty = 0.57$, pressure recovery is higher and distortion is lower for the present than for the previous inlet. In fact, at all reduced mass-flow ratios, pressure recovery is higher and distortion lower at a given mass flow ratio for the present inlet. At Mach numbers 0.95 and 1.0, the result is the same. (The two Mach numbers indicated are considered close enough for direct comparison.) At Mach numbers 1.1 to 1.4 (fig. 27(b)), direct comparisons are not made because of the differences in test Mach numbers.

CONCLUDING REMARKS AND RECOMMENDATIONS

A large-scale model of an axisymmetric inlet system was tested from Mach numbers 0.8 to 2.65. The inlet bleed system was designed using a relatively new design procedure (ref. 1). The inlet performance was measured at Mach number 2.65 with the predicted bleed configuration and a number of variations. Additionally, different vortex generator configurations were investigated at Mach numbers 2.65 and 2.50. The performance was compared with predictions and with the performance of a previous inlet system with the same internal contours but with a bleed system developed by "cut and try" methods in the wind tunnel. The important results from this investigation are discussed below.

Inlet With the Predicted Bleed Configuration

1. At critical conditions at Mach number 2.65, total-pressure recovery at the engine face was 93 percent with a bleed mass-flow ratio of 0.075 and a total-pressure distortion less than 10 percent. Small changes to this bleed system caused only small performance changes.

2. Experimentally measured bleed-mass flows were in good agreement with analytic predictions, as evidenced by results at Mach number 2.65 which show that the change in bleed mass-flow ratio from a supercritical to the critical operating condition was only 0.004 less than the predicted change of 0.023.

3. "Gaps" in the schedule for the forward centerbody bleed system caused relatively poor performance and terminal shock wave instability at centerbody positions where a "gap" prevented bleed. Performance was improved by a simple alteration of the bleed schedule which removed these "gaps" (see fig. 4).

4. Vortex generators on both cowl and centerbody gave the best performance at Mach numbers 2.65 and 2.50.

5. There were "open but inactive" bleed holes in the supersonic diffuser which caused performance penalties at Mach number 2.65.

Performance Comparison With the Inlet Having a Bleed System Developed With "Cut and Try" Methods

6. At critical conditions at Mach number 2.65, total-pressure recovery and the bleed mass-flow ratio were higher for the inlet with the "cut and try" bleed system. However, over a range of supercritical operation from bleed mass flow ratios of 0.055 to 0.065, total-pressure recovery was higher for the inlet with the "predicted bleed" configuration.

7. At off-design supersonic Mach numbers, pressure recovery was higher and the bleed mass-flow ratio generally about the same for the inlet with the "cut and try" bleed system. Distortion was high for both inlets.

8. At transonic Mach numbers and a constant mass-flow ratio at the engine face, pressure recovery was higher and distortion lower for the inlet with the "predicted" bleed configuration.

9. No differences in performance were found that could be traced to the difference in size of the bleed holes.

10. No single configuration of vortex generators was found for either inlet model that reduced the total-pressure distortion at the engine face to an acceptable level throughout the Mach number range.

Recommendations

The results of this and the previous investigation (ref. 3) revealed some weaknesses in the bleed system design procedure as well as some areas for inlet performance improvement not covered by the analytic methods. Some of the recommendations are listed below.

1. The methods for computation of the boundary layer underpredict the boundary-layer thickness and overpredict the pitot pressures within the boundary layer (fig. 25). Therefore, better methods for these computations are needed, contrary to the conclusions of reference 2.

2. Additional data are needed on the performance of bleed holes to permit realization of the full benefits of the bleed system design procedures used in this study. In particular, there are insufficient data on the effort of hole size, hole slant angle, and the ratio of hole length to diameter. In addition, the effect of approach boundary layer on the flow coefficients needs to be determined.

3. Traveling bleed systems should be designed to provide boundary-layer removal continuously as a function of the centerbody position. For example, gaps which are present in the forward bleed schedule (fig. 4) should be avoided.

4. The forward bleed region should be active at all centerbody positions as they were for the inlet of reference 3 (see fig. 20) because open but inactive holes in the supersonic diffuses caused performance penalties (see fig. 18).

5. As the terminal shock wave moves from an operating to a critical condition, the increase in bleed mass flow and hence the inlet stability margin would be greater if a larger area of the porous wall is affected. This possibility would be enhanced if the forward bleed (fig. 19) were located closer to the throat bleed regions and if not too great a portion of the boundary layer is removed in the upstream bleed regions. This modification would allow the effect of the pressure rise at the terminal shock wave to feed forward of the terminal shock location.

6. The best vortex generator configuration might be a system that could be "weathervaned" in supersonic flow and pitched mechanically in subsonic flow where the generators do reduce distortion.

Ames Research Center
National Aeronautics and Space Administration
Moffett Field, Calif., 94035, Jan. 9, 1973

REFERENCES

1. Reyhner, Theoredore A.; and Hickcox, Timothy E.: A Procedure for Combined Viscous-Inviscid Analysis of Supersonic Inlet Flow Fields. Presented at AIAA 10th Aerospace Sciences Meeting, San Diego, California, Paper 72–44, Jan. 17–19, 1972.

2. Koncsek, J. L.; and Syberg, J.: Transonic and Supersonic Test of Mach 2.65 Mixed-Compression Axisymmetric Intake. NASA CR–1977, 1972.

3. Smeltzer, Donald B.; and Sorensen, Norman E.: Tests of a Mixed Compression Axisymmetric Inlet With Large Transonic Mass Flow at Mach Numbers 0.6 to 2.65. NASA TN D–6971, 1972.

4. Sorensen, Virginia L.: Computer Program for Calculating Flow Fields in Supersonic Inlets. NASA TN D–2897, 1965.

5. Syberg, J.; and Koncsek, J. L.: Transonic and Supersonic Test of the SST Prototype Air Intake. Rept. No. FAA–SS–72–50, The Boeing Co., Apr. 1972.

6. McLafferty, G.; and Ranard, E.: Pressure Losses and Flow Coefficients of Slanted Perforations Discharging From Within a Simulated Supersonic Inlet. Rept. R–0920–1, United Aircraft Corporation Research Department Dec. 9, 1958.

7. Tjonneland, E.: The Design, Development, and Testing of a Supersonic Transport Inlet System. Presented at NATO 38th Meeting of AGARD Propulsion and Energetic Panel, Sandefjord, Norway, Paper 18, Sept. 13–17, 1971.

TABLE 1.– INLET COORDINATES

Centerbody

x/R	r_{cb}/R
0	0
straight taper	
2.560	0.4055
2.650	.4202
2.750	.4367
2.850	.4540
2.950	.4721
3.050	.4907
3.150	.5103
3.250	.5301
3.350	.5509
3.450	.5721
3.550	.5940
3.650	.6140
3.700	.6218
3.750	.6278
3.800	.6329
3.850	.6370
3.900	.6407
3.950	.6437
4.000	.6460
4.050	.6477
4.088	.6481 ← $r_{cb_{max}}/R$

x/R	r_{cb}/R
4.125	0.6477
4.175	.6461
4.225	.6437
4.300	.6381
4.400	.6285
straight taper	
4.750	.5916
4.850	.5793
4.950	.5640
5.050	.5468
5.150	.5289
5.250	.5066
5.350	.4807
5.400	.4640
5.450	.4430
straight taper	
5.643	.3627
5.694	.3600
straight line	
6.489	.3600
straight line	
7.262	.3547

Cowl

x_c/R	r_c/R
0	1.0000
straight taper	
0.175	1.0046
.250	1.0062
.325	1.0073
.375	1.0077
.425	1.0078
.500	1.0074
.575	1.0062
.650	1.0042
.725	1.0011
.800	.9972
.875	.9921
.950	.9862
1.025	.9792
1.100	.9712
1.175	.9622
1.250	.9520
1.350	.9379
1.450	.9235
1.550	.9093
1.650	.8949
1.700	.8875
1.750	.8806
1.800	.8758
1.833	.8738
straight taper	
2.000	.8662

x_c/R	r_c/R
2.025	0.8652
2.050	.8647
2.075	.8645 } $r_{c_{min}}/R$
straight line	
2.175	.8645
2.275	.8655
2.475	.8700
2.675	.8760
2.875	.8821
3.075	.8905
3.175	.9001
3.375	.9295
3.575	.9582
3.675	.9675
3.775	.9733
3.875	.9766
3.984	.9786
bypass gap	
4.388	1.0090
4.389	1.0023
4.392	.9968
4.403	.9868
4.427	.9753
4.474	.9637
4.538	.9590
straight line	
4.937	.9590 ← engine face

TABLE 2.– CENTERBODY BLEED HOLES

Plenum	Row	Row location, x/R	Holes per row	Hole angle to surface, deg	Hole length to diameter, l/d
1	1	3.700	213	20	5.0
	2	3.732			
	3	3.764[a]			
	4	3.796[a]			
	5	3.828[a]			
	6	3.860[a]			
2	7	3.920	219	40	3.0
	8	3.934			
	9	3.948			
	10	3.976[a]			
	11	3.990[a]			
	12	4.004[a]			
3	13	4.048	220	40	3.0
	14	4.062			
	15	4.076			
	16	4.112[a]			
	17	4.126[a]			
	18	4.140[a]			
4	19	4.200[a]	300	90	1.8
	20	4.216[a]			
	21	4.232			
	22	4.248			
5	23	4.300[a]	300	90	1.8
	24	4.316[a]			
	25	4.332			
	26	4.348			
6	27	4.390[a]	296	90	1.8
	28	4.406[a]			
	29	4.422			
	30	4.438			
7	31	4.490[a]	292	90	1.8
	32	4.506[a]			
	33	4.522			
	34	4.538			
8	35	4.580[a]	286	90	1.8
	36	4.596[a]			
	37	4.612			
	38	4.628			
9	39	4.680[a]	282	90	1.8
	40	4.696[a]			
	41	4.712			
	42	4.728			
10	43	4.770[a]	276	90	1.8
	44	4.786[a]			
	45	4.802			
	46	4.818			
11	47	4.860[a]	268	90	1.8
	48	4.876[a]			
	49	4.892			
	50	4.908			
12	51	4.950[a]	262	90	1.8
	52	4.966[a]			
	53	4.982			
	54	4.998			
13	55	5.040[a]	256	90	1.8
	56	5.056[a]			
	57	5.072			
	58	5.088			
14	59	5.130[a]	247	90	1.8
	60	5.146[a]			
	61	5.162			
	62	5.178			
15	63	5.220[a]	237	90	1.8
	64	5.236[a]			
	65	5.252			
	66	5.268			
16	67	5.310[a]	226	90	1.8
	68	5.326[a]			
	69	5.342			
	70	5.358			
17	71	5.390[a]	211	90	1.8
	72	5.406[a]			
	73	5.422			
	74	5.438			

Note: d/R = 0.00639 for all holes

[a]Rows open, predicted bleed configuration

TABLE 3.– COWL BLEED HOLES

Plenum	Row	Row location, x_c/R	Holes per row	Hole angle to surface, deg	Hole length to diameter, l/d
1	1	1.275	273	20	5.0
	2	1.307			
	3	1.339			
	4	1.371			
	5	1.403			
	6	1.435[a]			
	7	1.467[a]			
	8	1.499			
	9	1.531			
	10	1.563[a]			
	11	1.595[a]			
2	12	1.675	360	40	3.0
	13	1.685			
	14	1.715[a]			
	15	1.725[a]			
	16	1.755[a]			
	17	1.765			
3	18	1.825	400	90	1.8
	19	1.835			
	20	1.845[a]			
	21	1.855[a]			
	22	1.865[a]			
	23	1.875[a]			
	24	1.885[a]			
	25	1.895[a]			
	26	1.905[a]			
	27	1.915			
	28	1.925			
	29	1.935			
	30	1.945			
	31	1.955			
	32	1.965			

Note: d/R = 0.00639 for all holes

[a]Rows open, predicted bleed configuration

TABLE 4.– VORTEX GENERATOR CONFIGURATIONS

Centerbody

Designation	Station, X/R	Size		No. of pairs	Spacing, a/b
		H/R	L/R		
Aft	4.77	.0511	.1022	12	2.3
Forward	4.62	.0511	.1022	12	2.3

← Initial configuration

Cowl

Designation	Station, X_C/R	Size		No. of pairs	Spacing, a/b
		H/R	L/R		
Small	2.315	.0306	.0613	32	2.0
Large	2.315	.0511	.1022	24	1.67

← Initial configuration

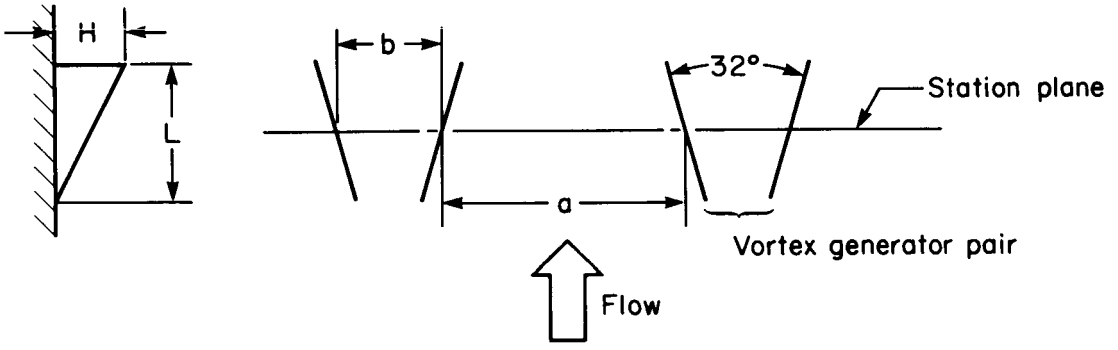

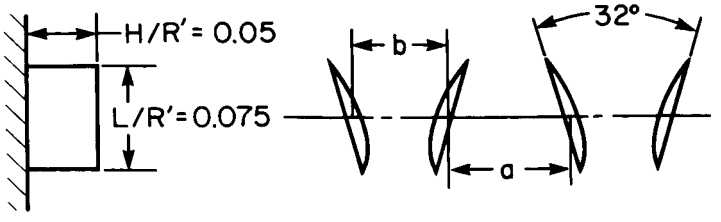

	Station	No. of pairs	a/b
Centerbody	X/R' = 4.75	24	1.0
Cowl	X_C/R' = 2.325	34	1.0

Previous inlet model (ref. 1)

TABLE 5.– MODEL CONFIGURATION PARAMETERS

Configuration	Bleed schedule	Open rows of bleed holes																			Bleed exit areas, $\frac{A_{exit}}{Ac}$					Vortex generators	
		Centerbody plenum																	Cowl plenum			Centerbody		Cowl				
		1	2	3	4	5	6	7	8	9	10	11	12	13	14	15	16	17	1	2	3	Forward	Throat	1	2	3	Center-body	Cowl
1	Predicted	3,4,5,6	10,11, 12	16,17, 18	19,20	23,24	27,28	31,32	35,36	39,40	43,44	47,48	51,52	55,56	59,60	63,64	67,68	71,72	6,7, 10,11	14,15, 16	20,21,22,23, 24,25,26	.0338	.0160	.0240	.0172	.0224	aft	small
2	Modified																											
3			8,9, 11,12																									
4		4,5,6																										
5			9,10, 11,12																									
6		3,4, 5,6																										
7																			8,9, 10,11		18,19,20,21, 22,23,24							
9																								.0173				
10																												LARGE
11																						.0405						
13																											FOR-WARD	
14																						.0270						
15																						.0338						
16																												NONE
17				NONE																								
18				16,17, 18																		.0405						

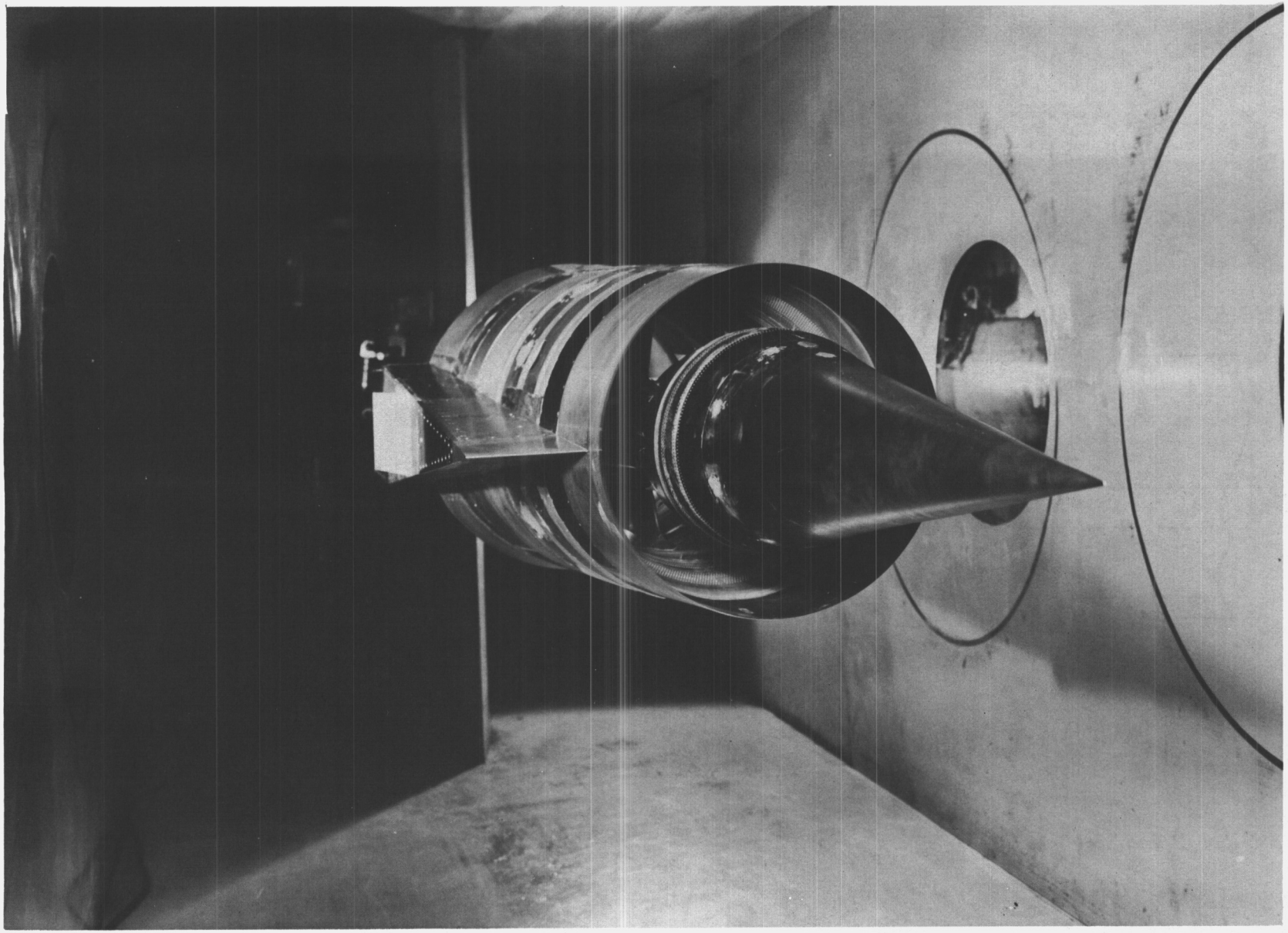

Figure 1.- Model mounted in the wind tunnel.

*Design position at $M_\infty = 2.65$

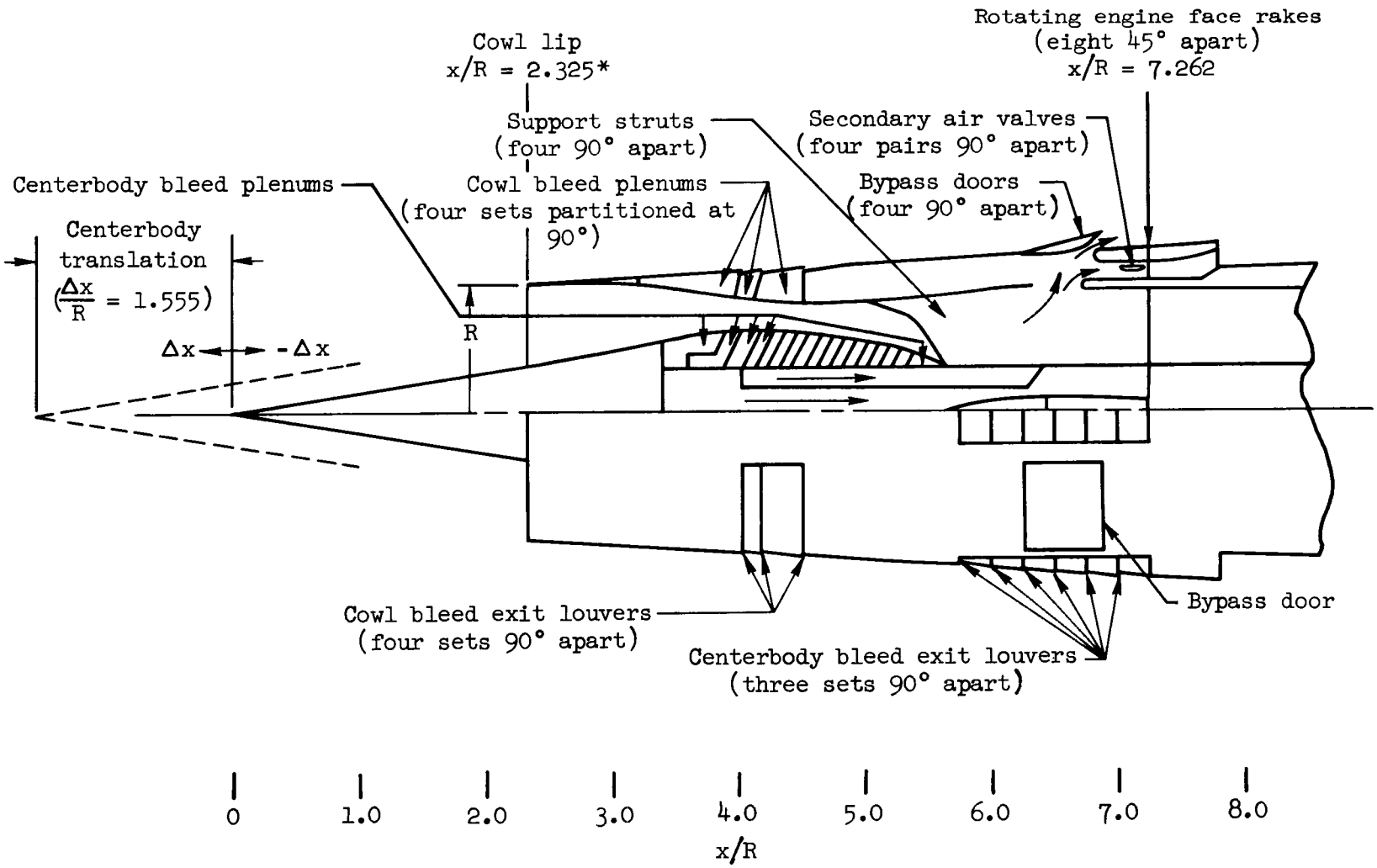

Figure 2.- Model.

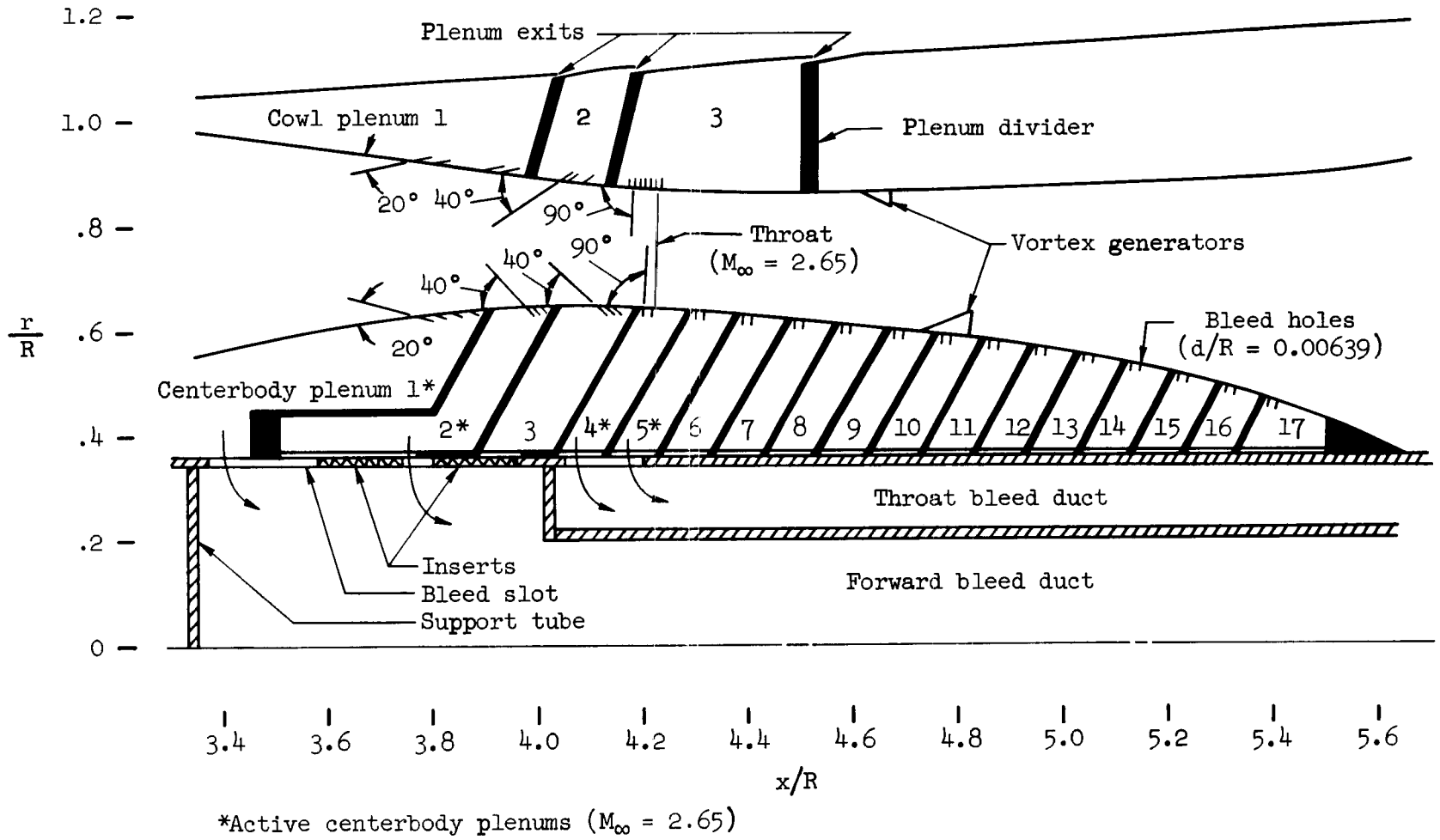

Figure 3.- Predicted bleed and vortex generator configuration, configuration 1; $\Delta x/R = 0$.

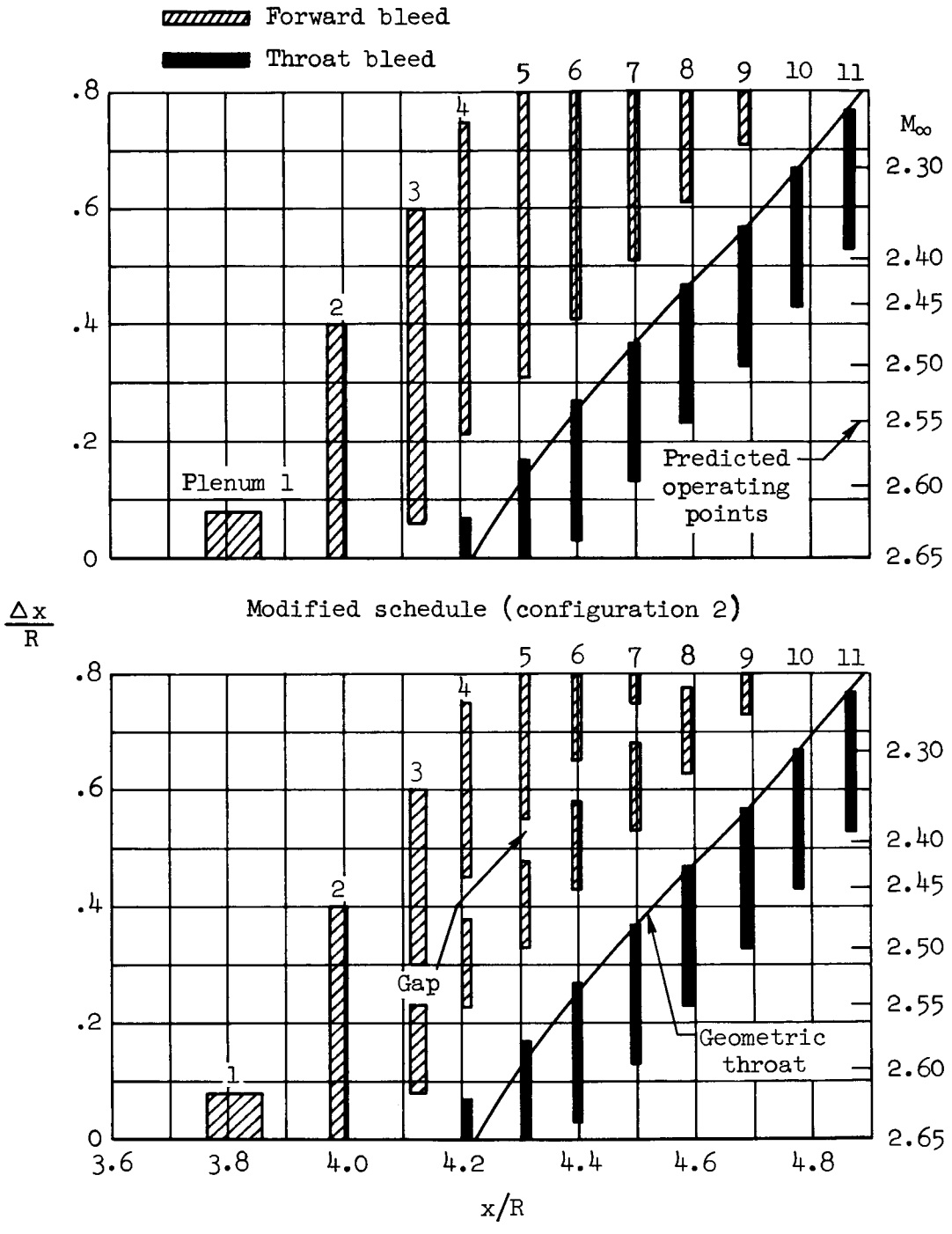

Figure 4.- Centerbody bleed schedules.

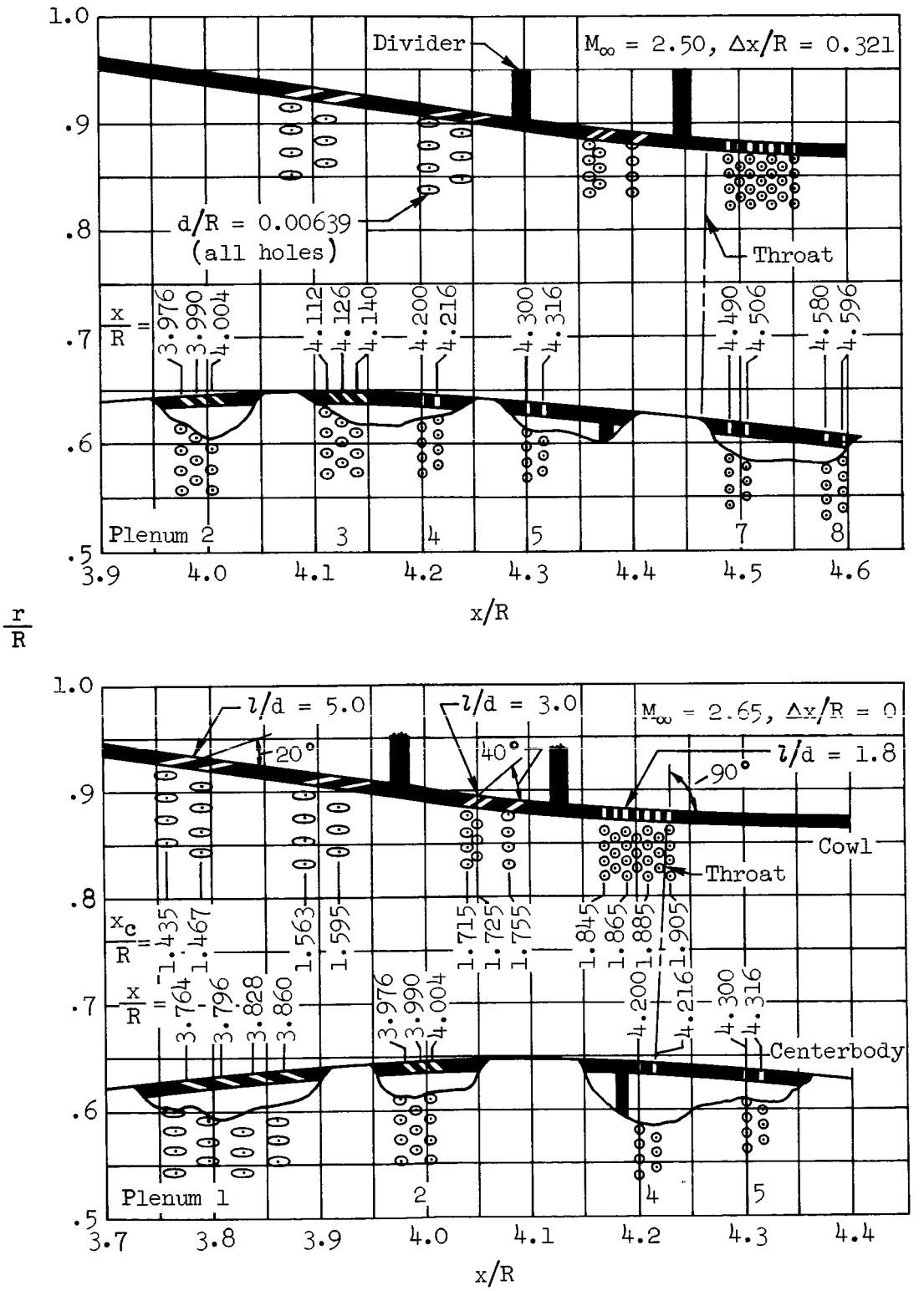

Figure 5.- Predicted bleed configuration, modified schedule (configuration 2).

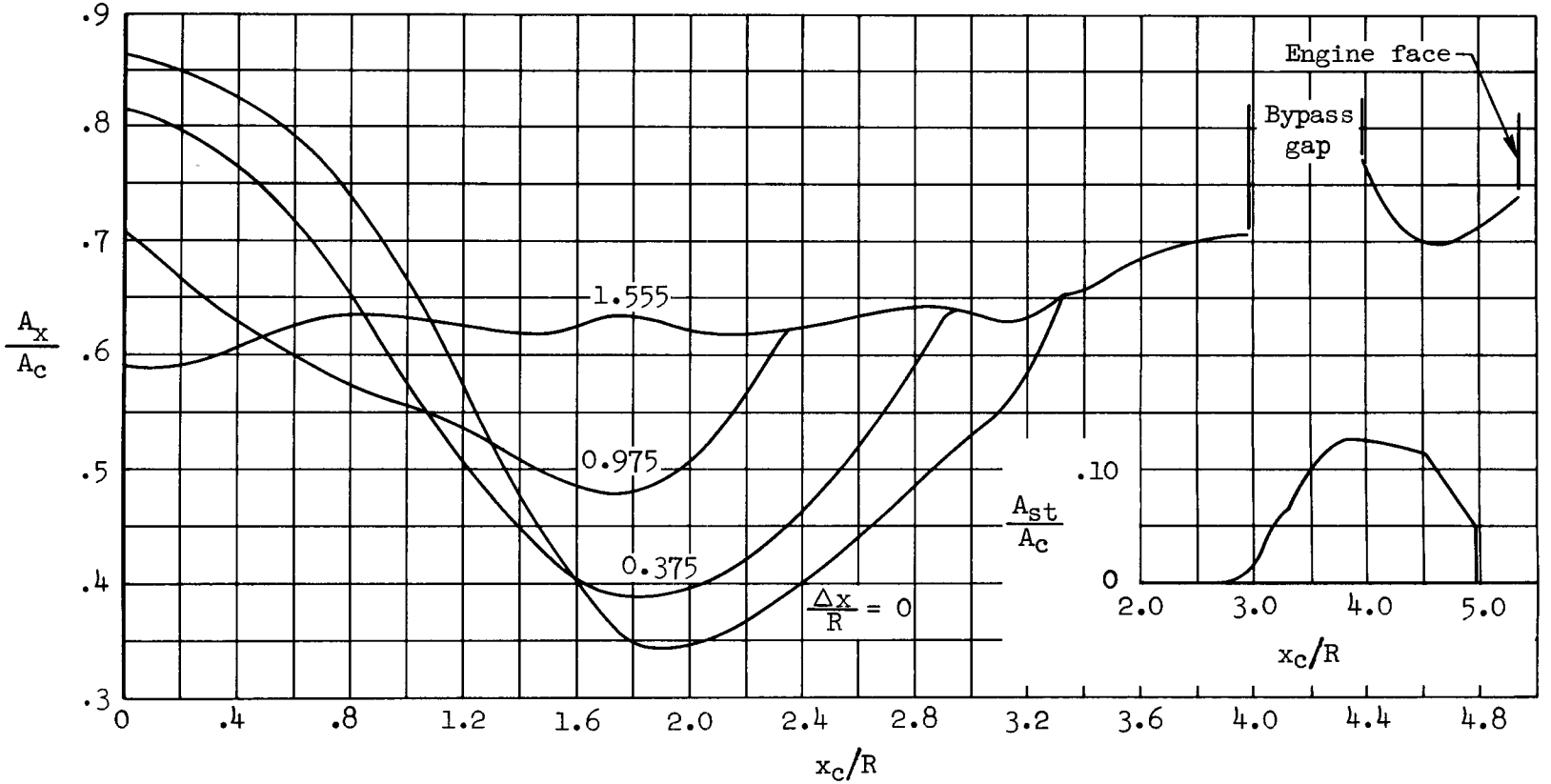

Figure 6.- Area distribution.

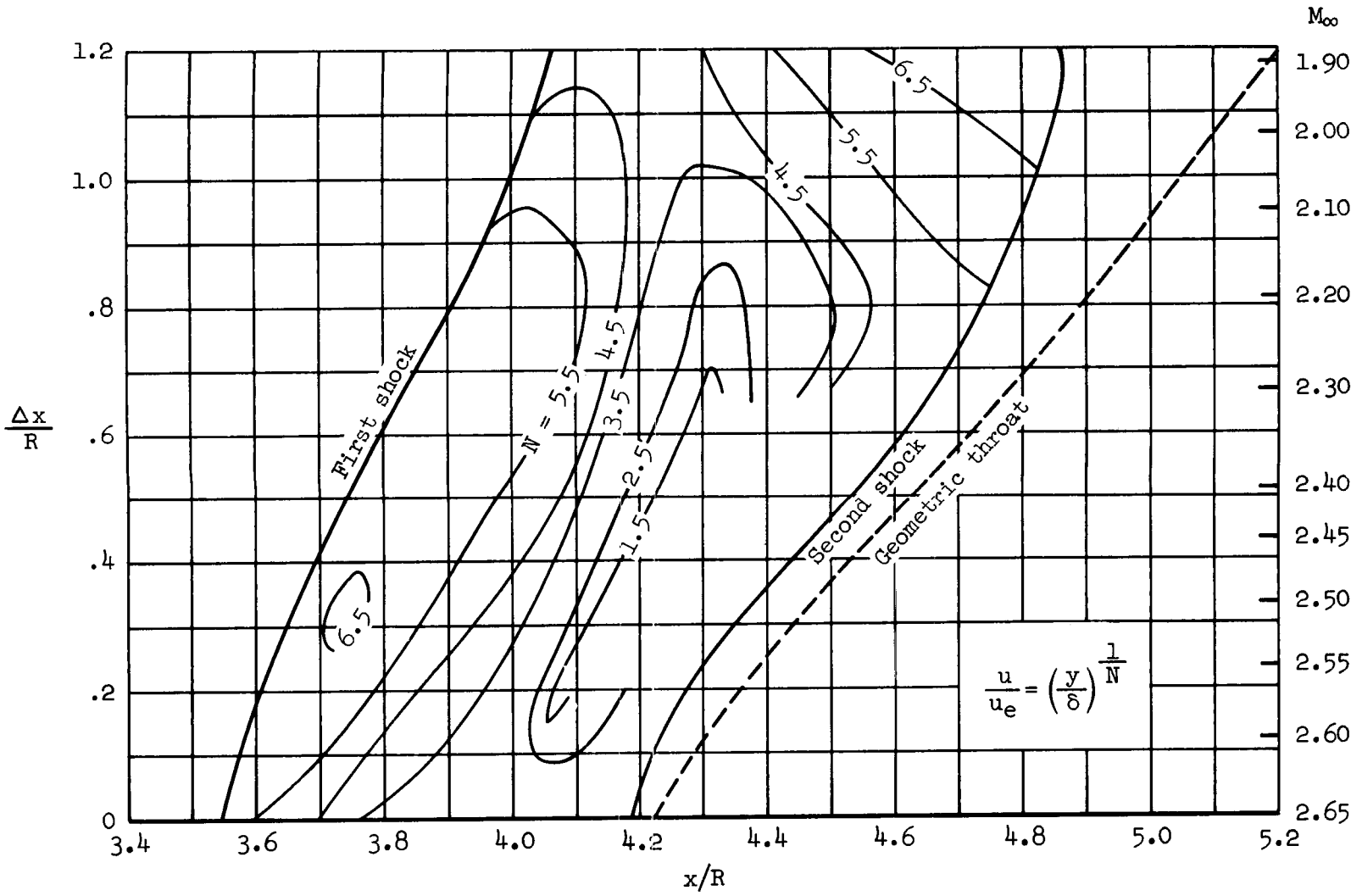

Figure 7.- Centerbody boundary-layer power law exponent, N.

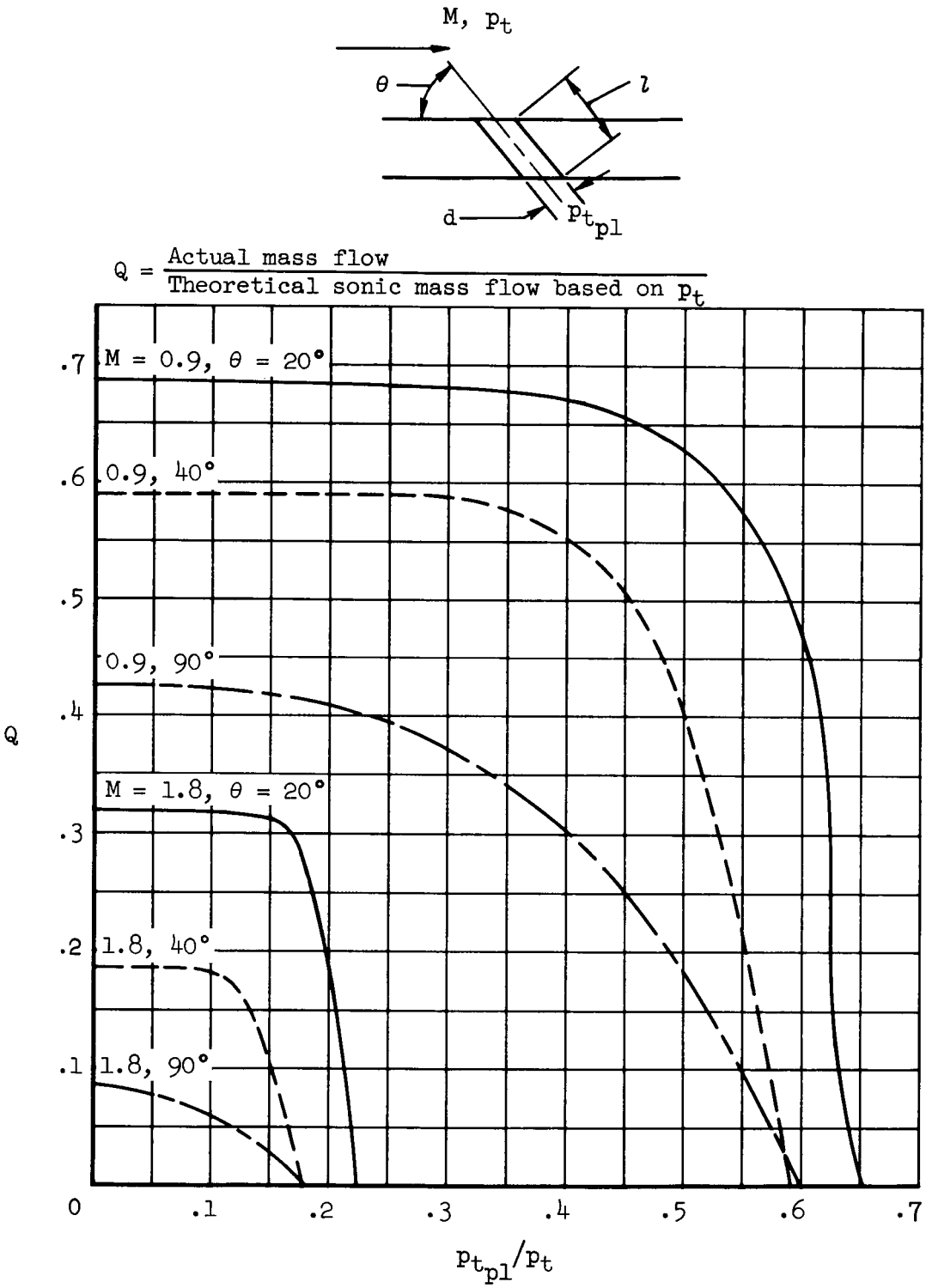

Figure 8.- Circular bleed hole performance; $l/d = 3$.

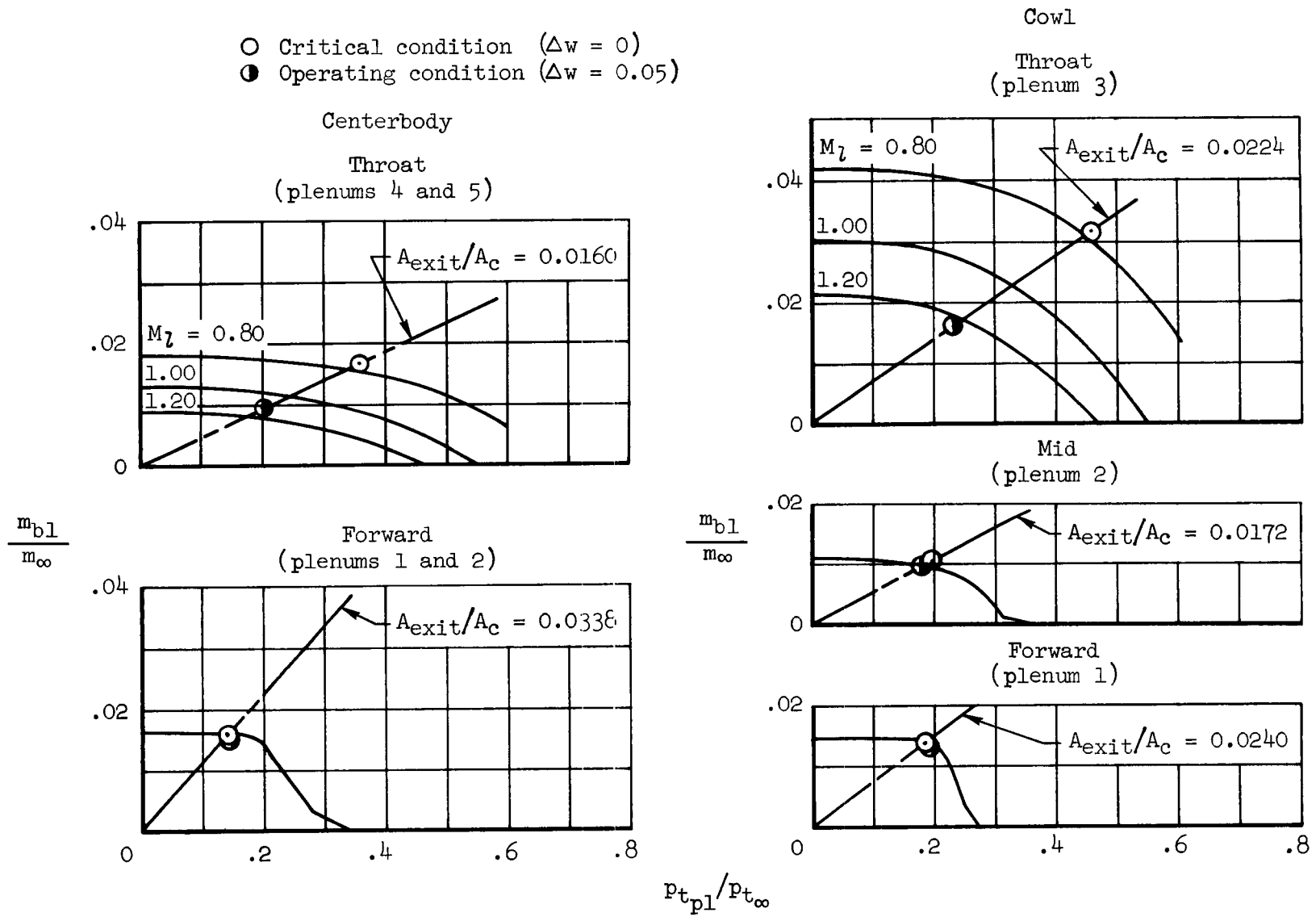

Figure 9.- Predicted performance of the bleed system; $M_\infty = 2.65$, $\alpha = 0°$.

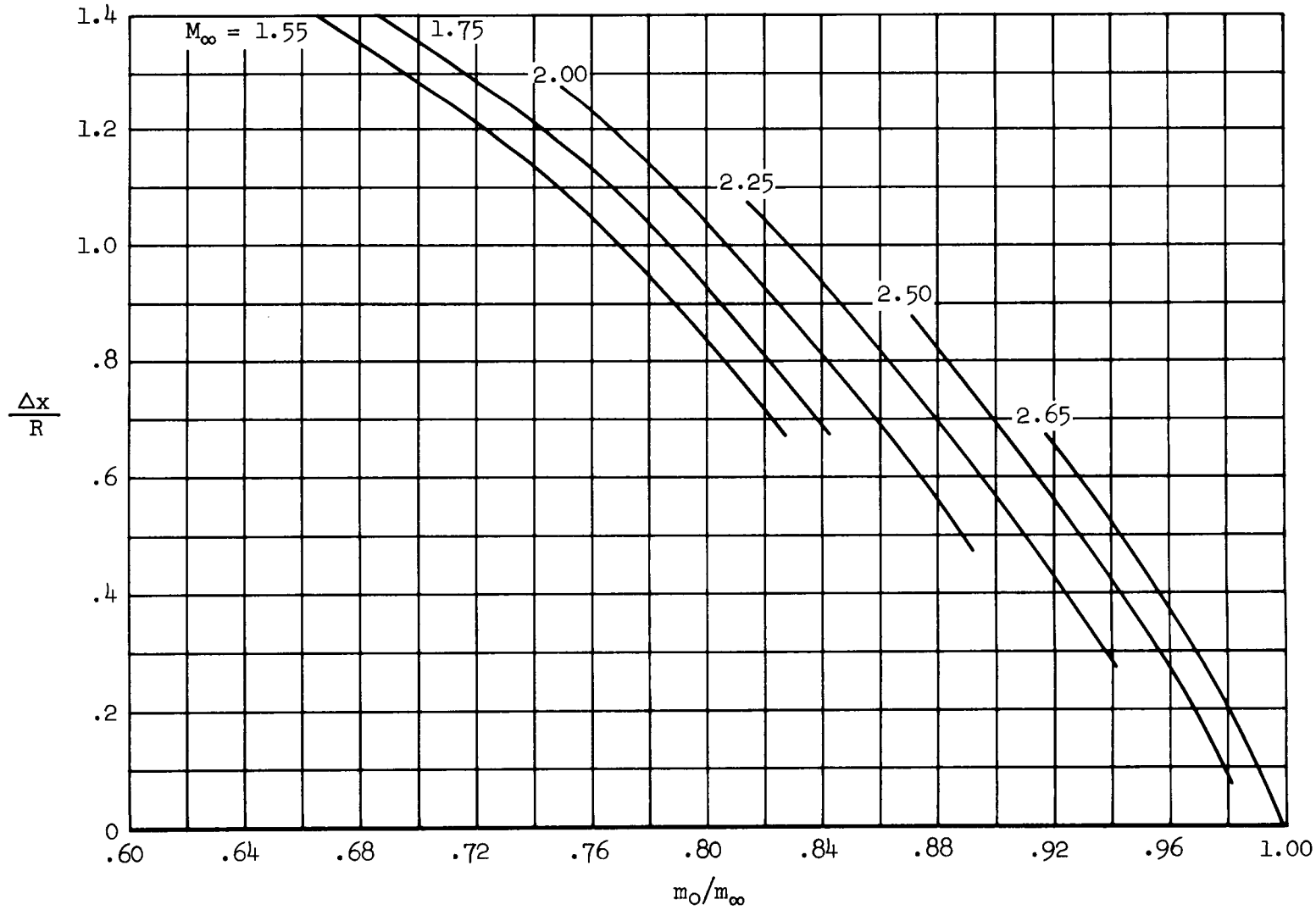

Figure 10.- Inlet capture mass flow ratio; $\alpha = 0°$.

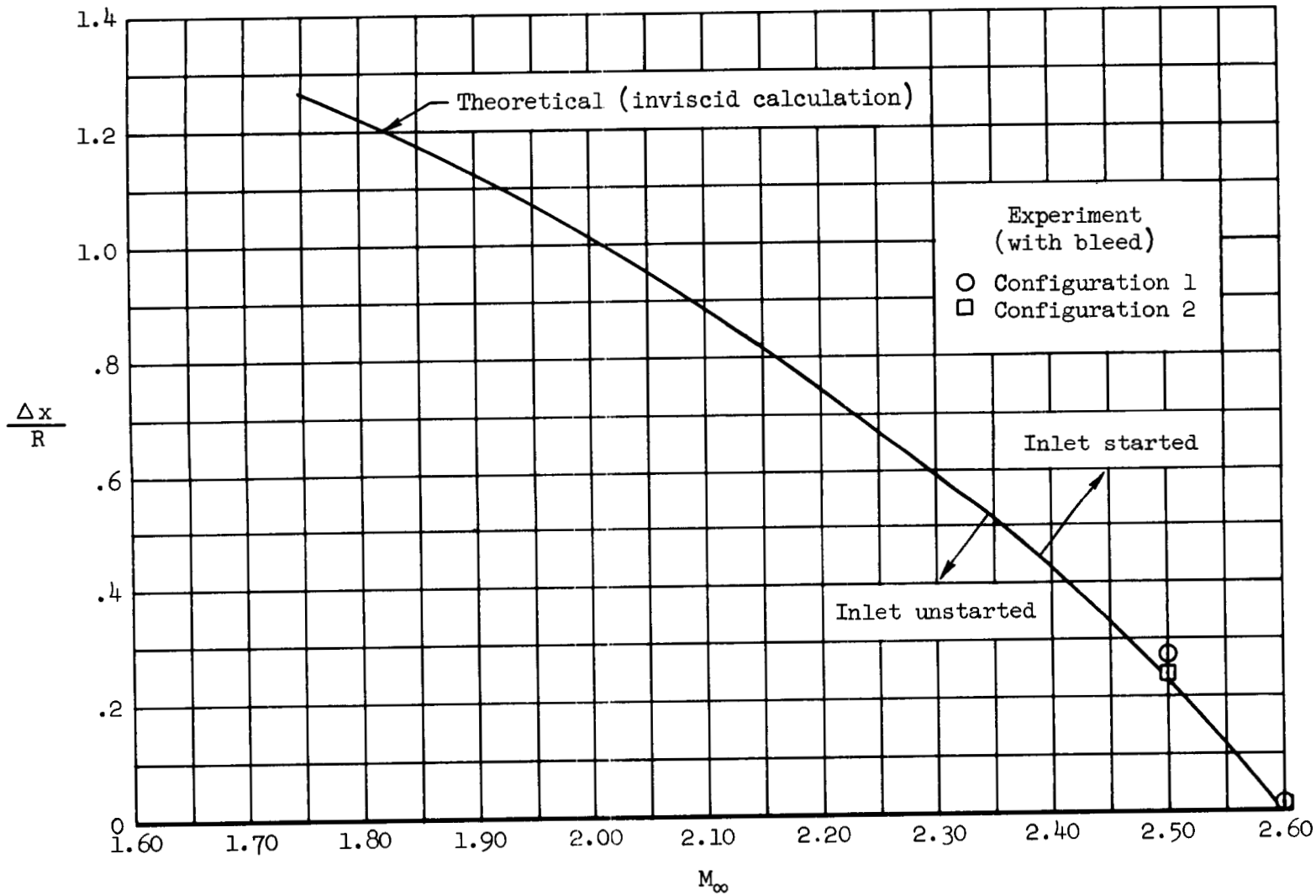

Figure 11.- Critical centerbody positions.

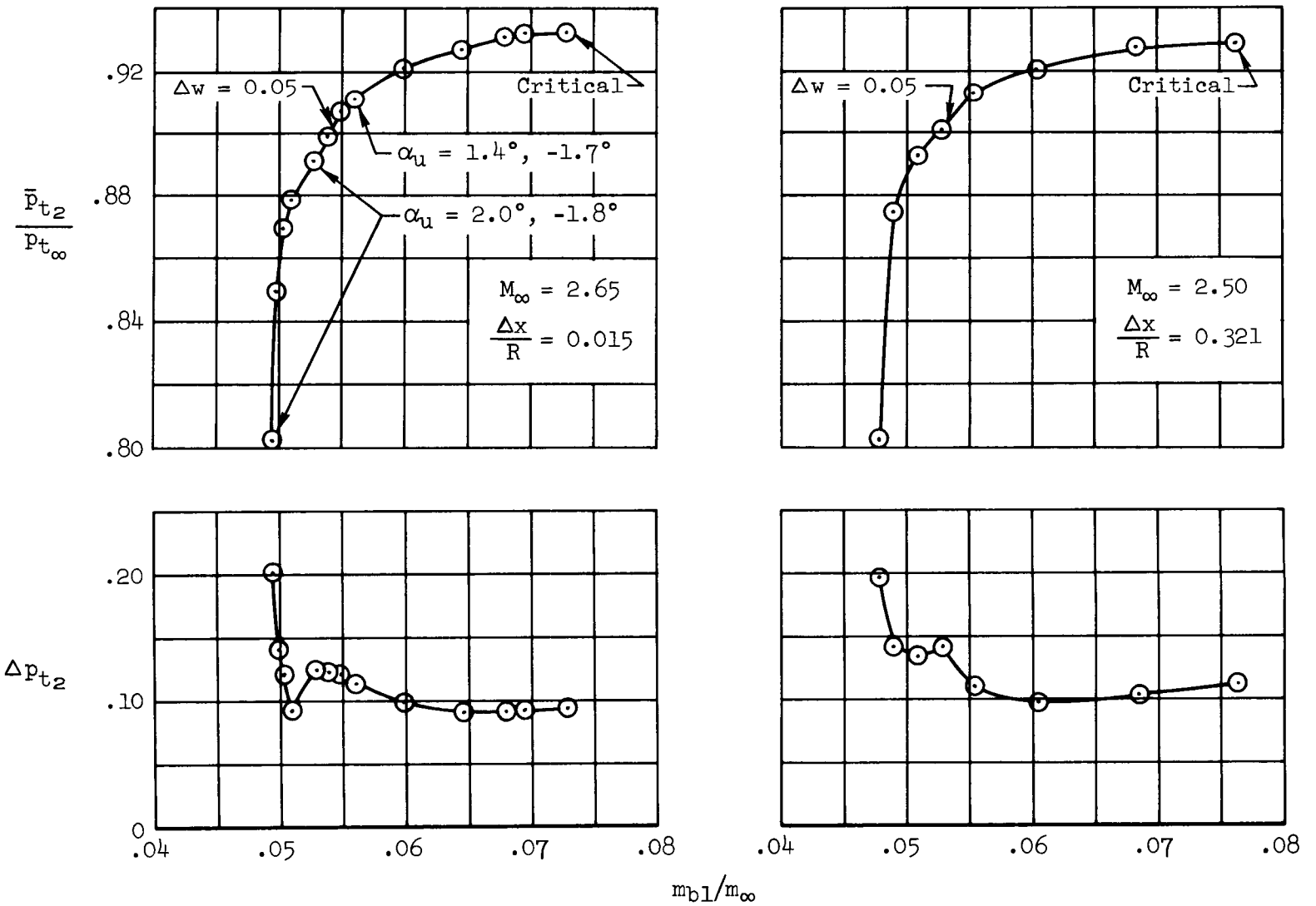

Figure 12.- Supercritical performance, configuration 2; $\alpha = 0°$.

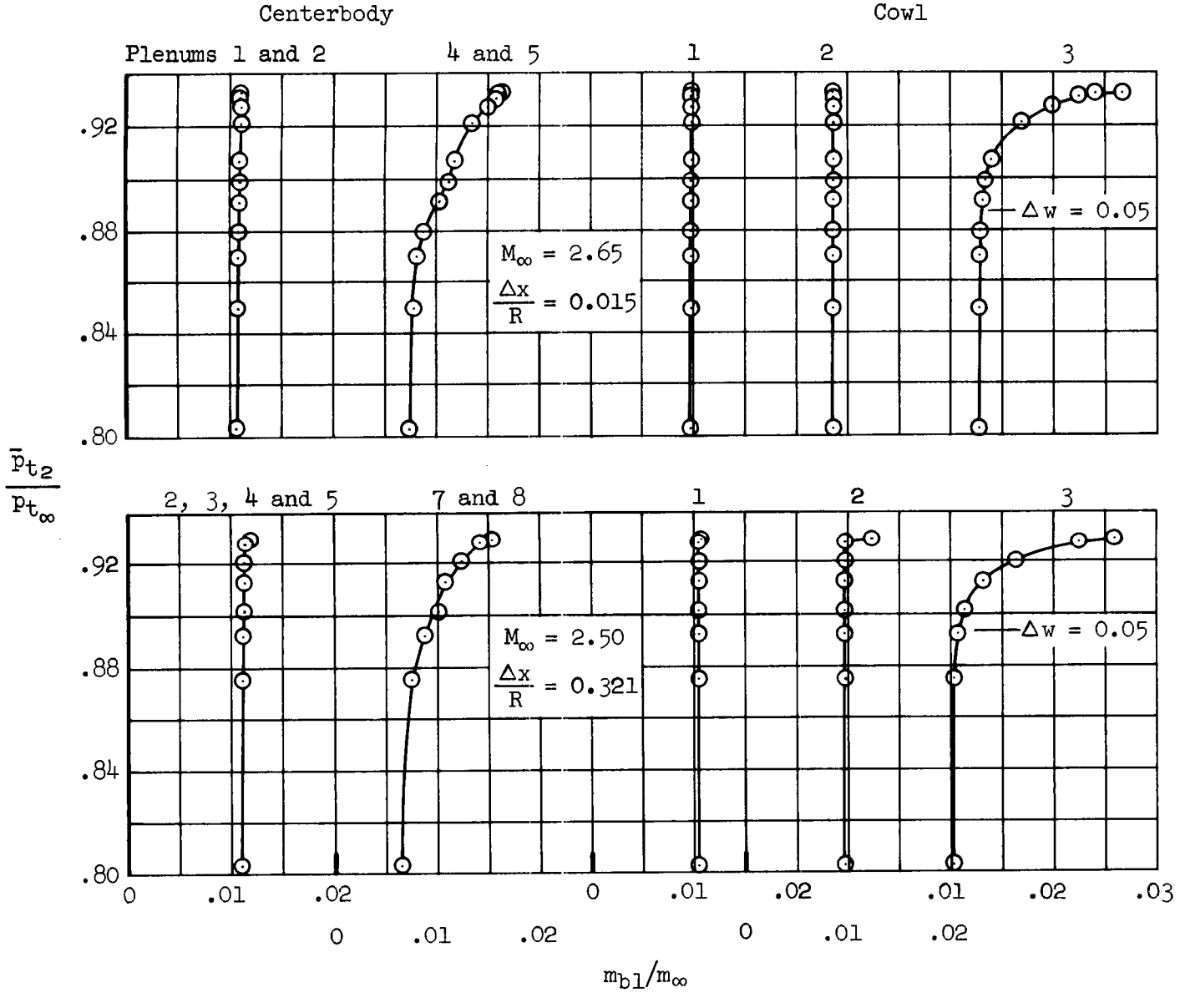

Figure 13.- Supercritical bleed flow in the individual plenums, configuration 2; $\alpha = 0°$.

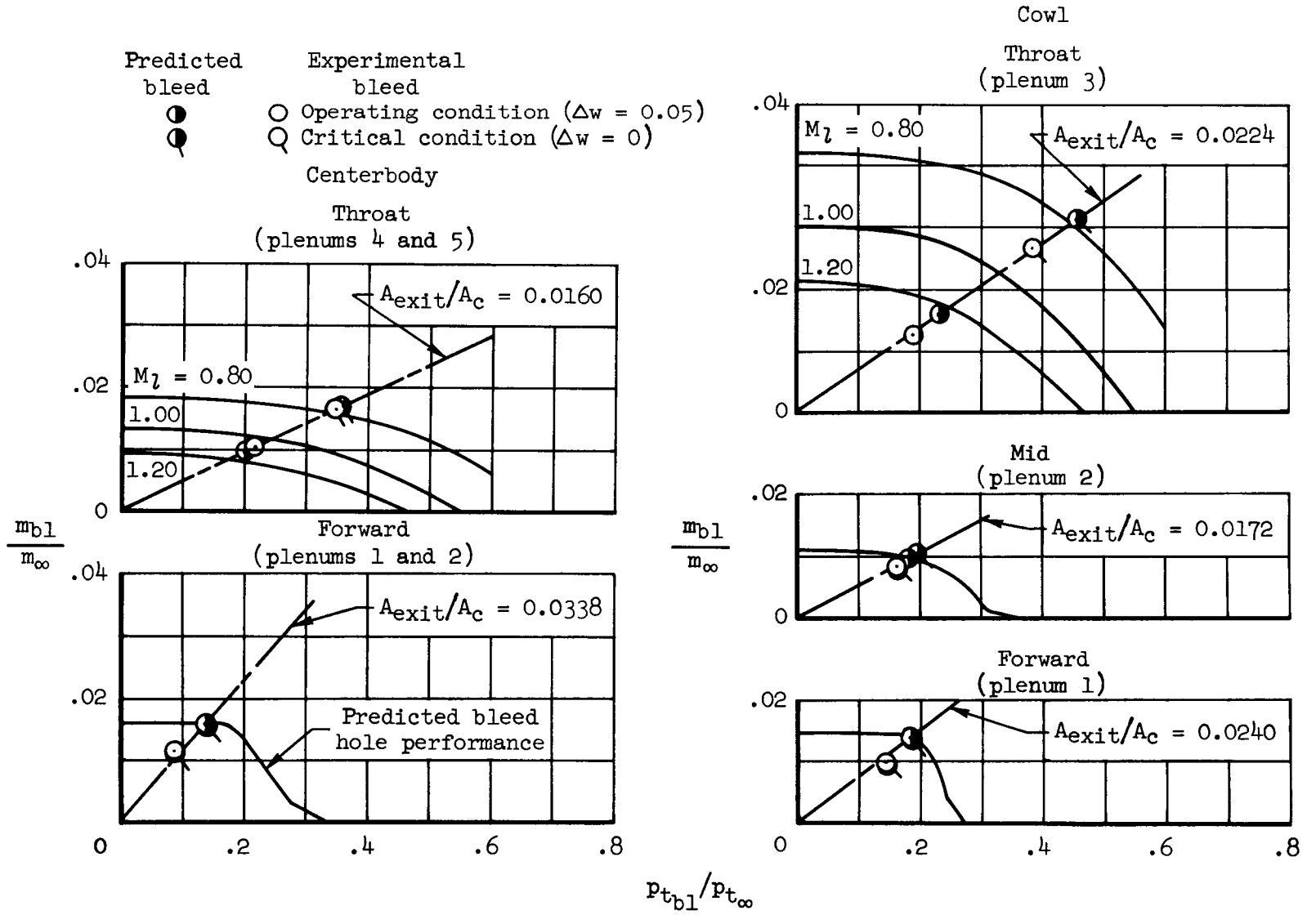

Figure 14.- Predicted and experimental bleed mass flow; $M_\infty = 2.65$, $\alpha = 0°$.

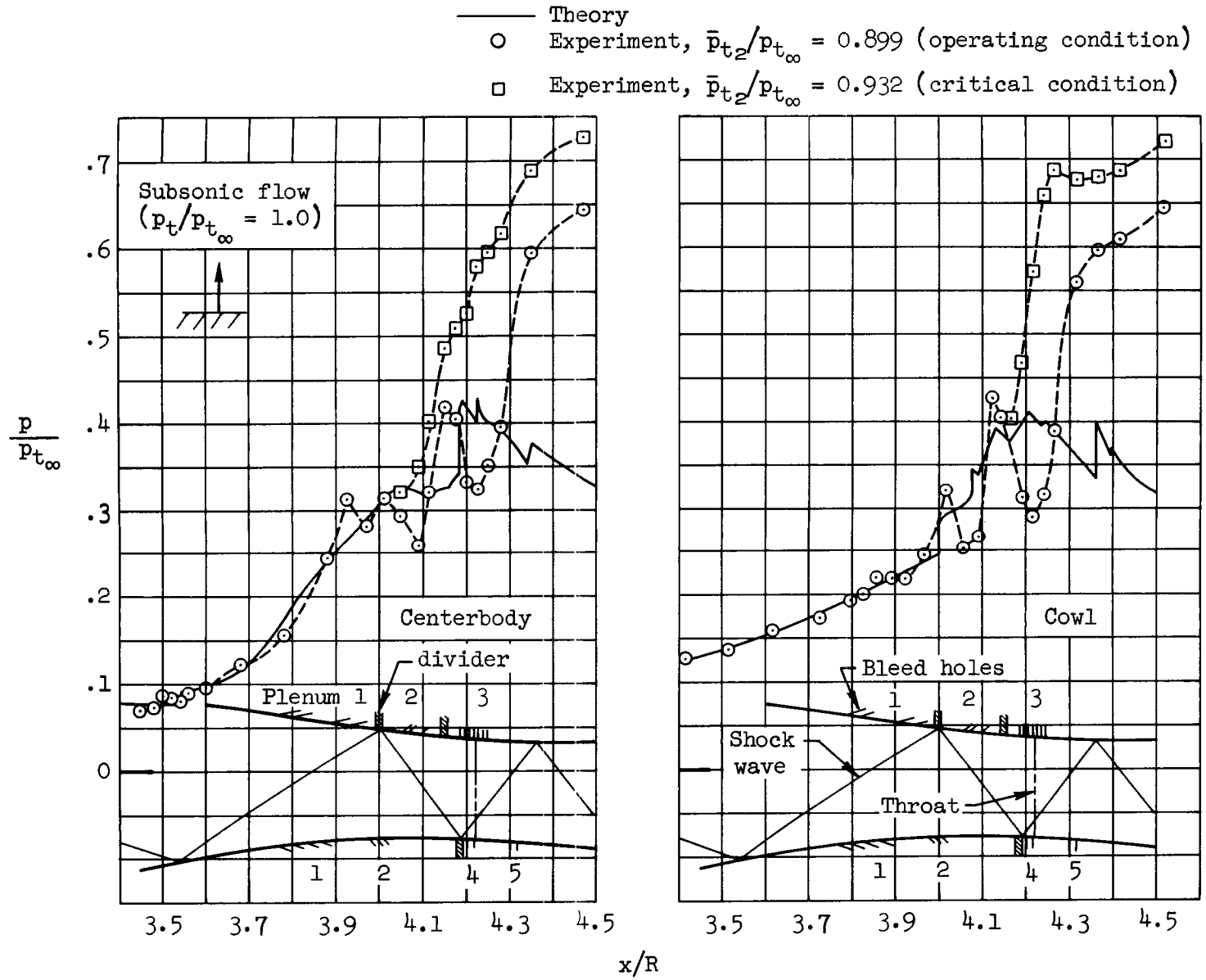

Figure 15.- Static pressure distributions, configuration 2; $M_\infty = 2.65$, $\alpha = 0°$, $\Delta x/R = 0.015$.

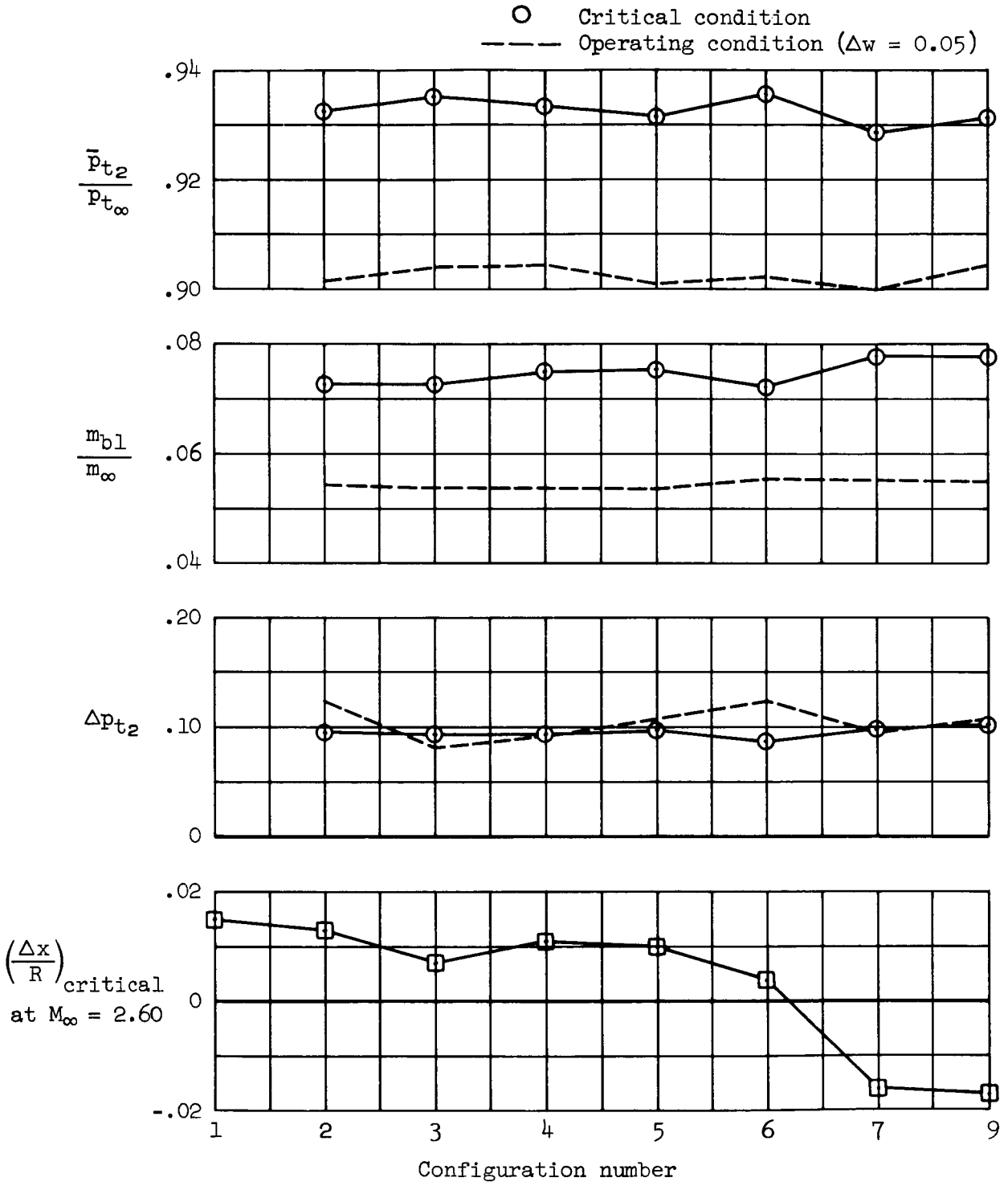

Figure 16.- Performance for various configurations, $M_\infty = 2.65$, $\alpha = 0°$, $\Delta M = 0.05$.

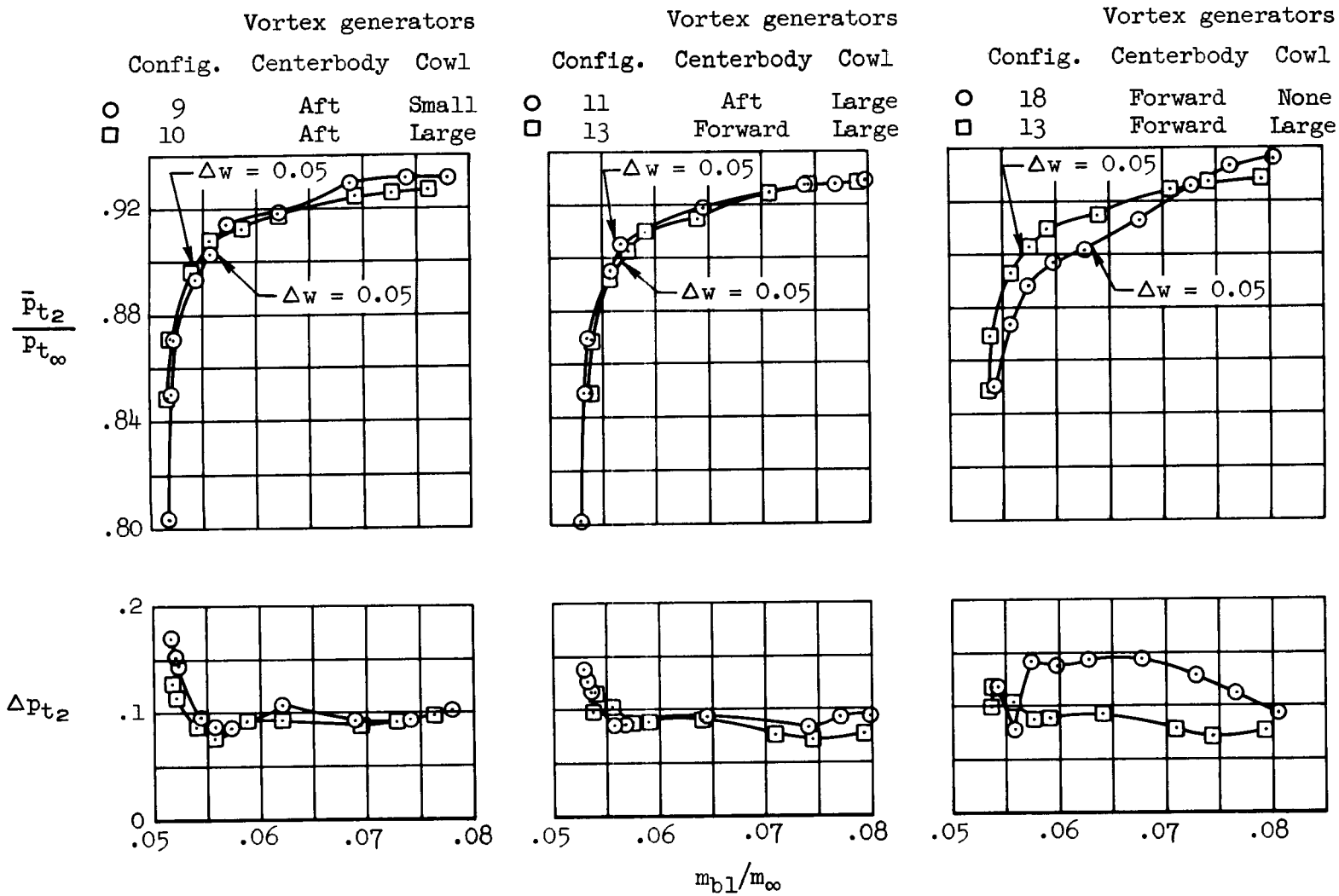

(a) $M_\infty = 2.65$

Figure 17.- Supercritical performance with various vortex generator configurations; $\alpha = 0°$, $\Delta M = 0.05$.

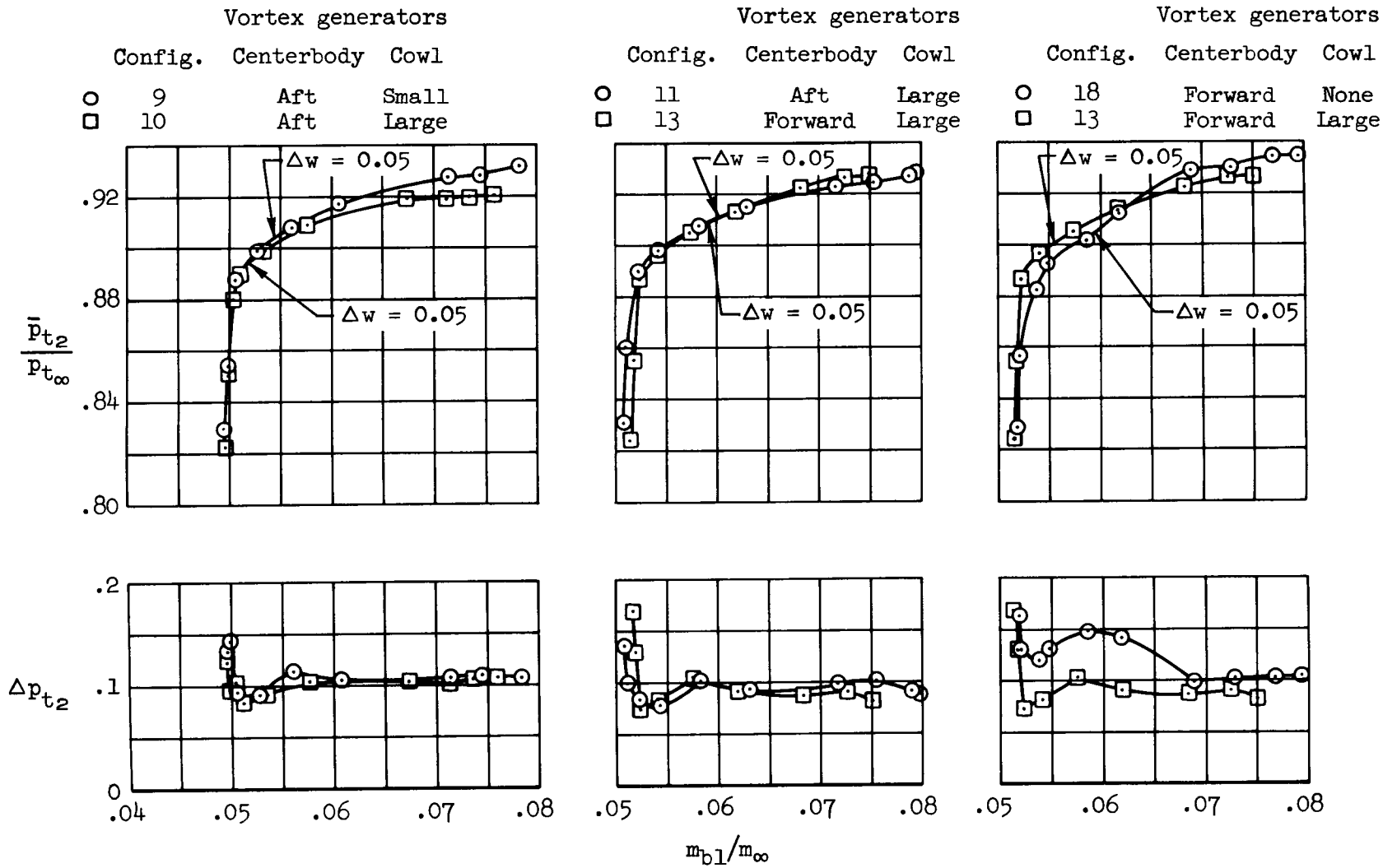

(b) $M_\infty = 2.50$

Figure 17.- Concluded.

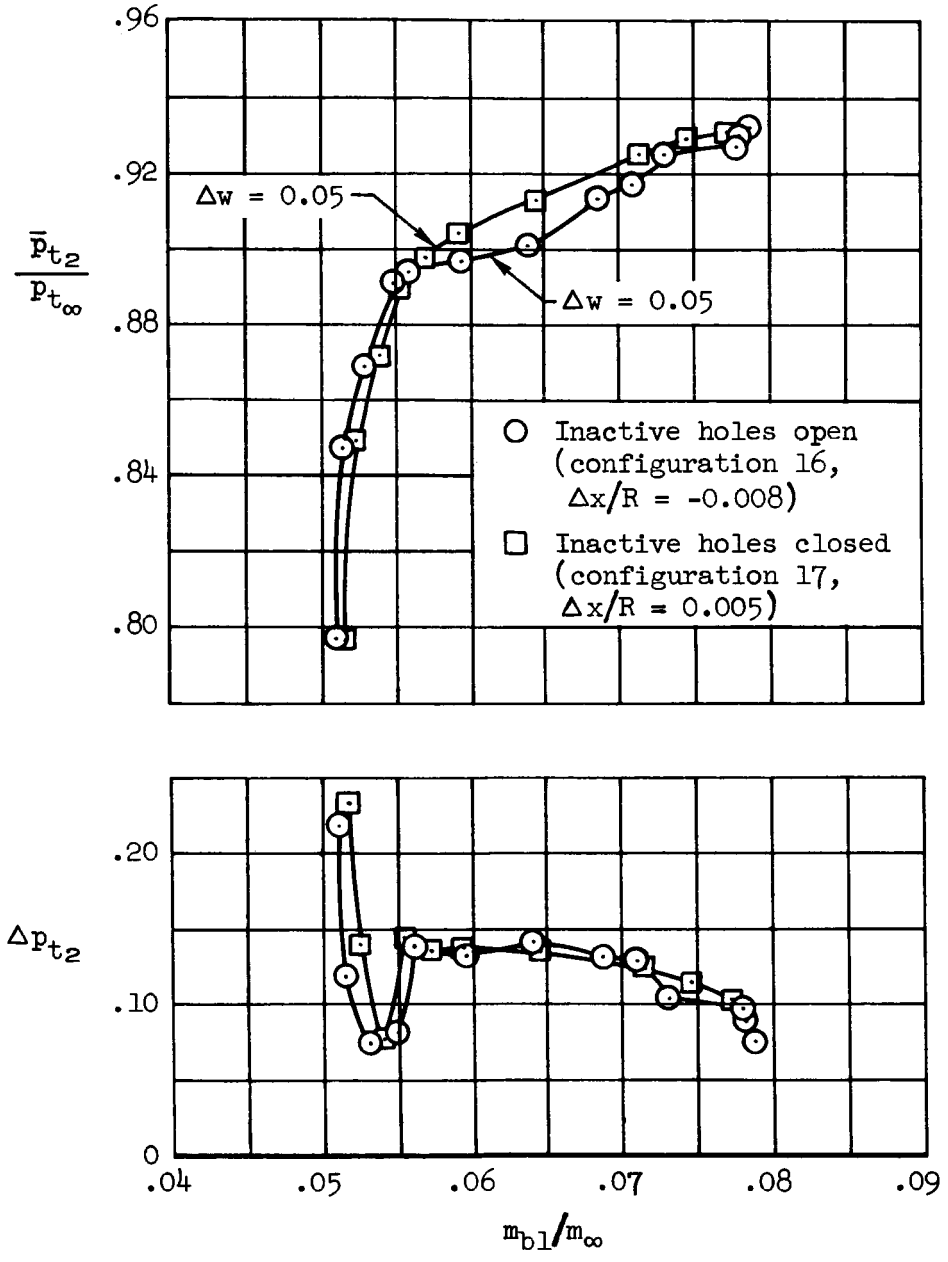

Figure 18.- Effect of centerbody plenum 3 bleed holes on the supercritical performance; $M_\infty = 2.65$, $\alpha = 0°$.

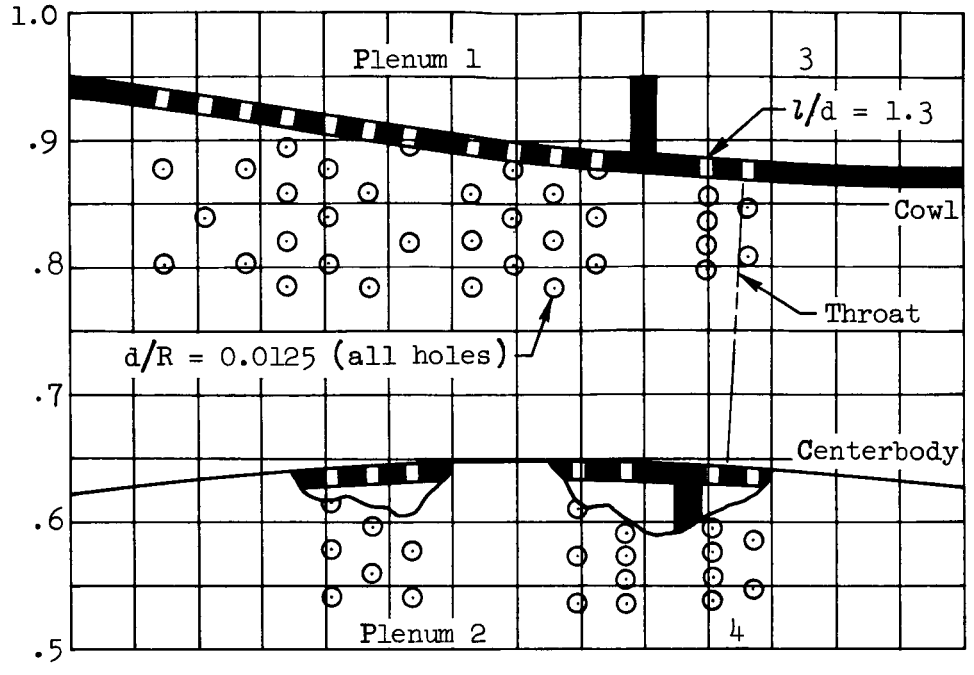

$\frac{r}{R}$

Configuration B-1 (previous inlet)

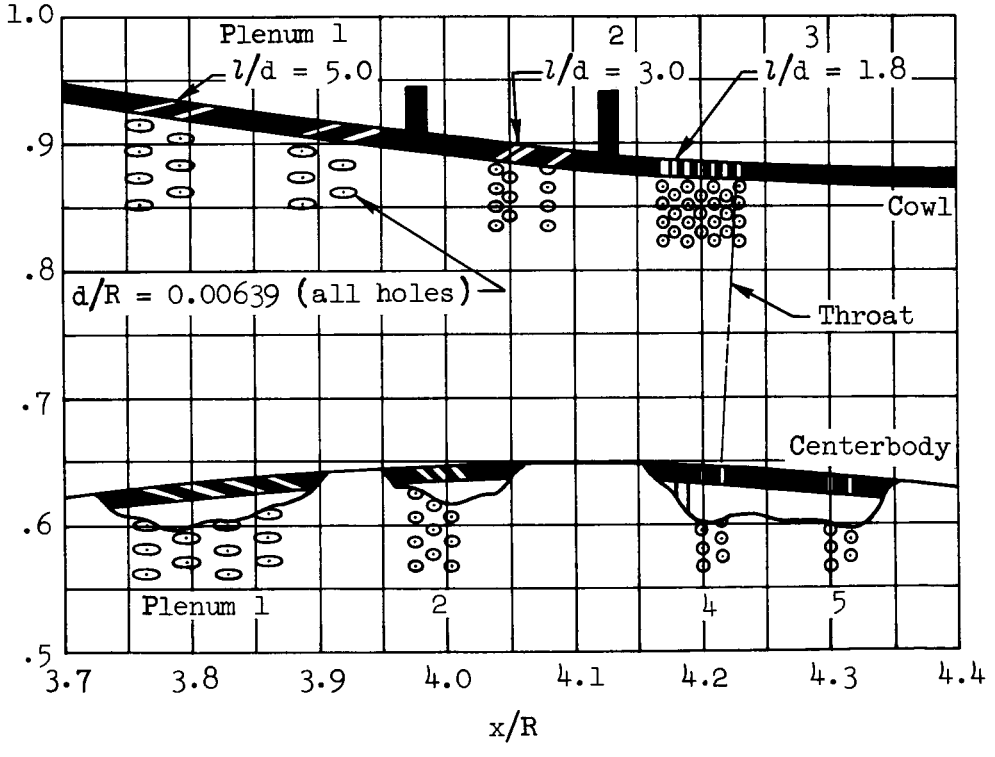

Configuration 2 (present inlet)

Figure 19.- Bleed configuration comparison; $\Delta x/R = 0$.

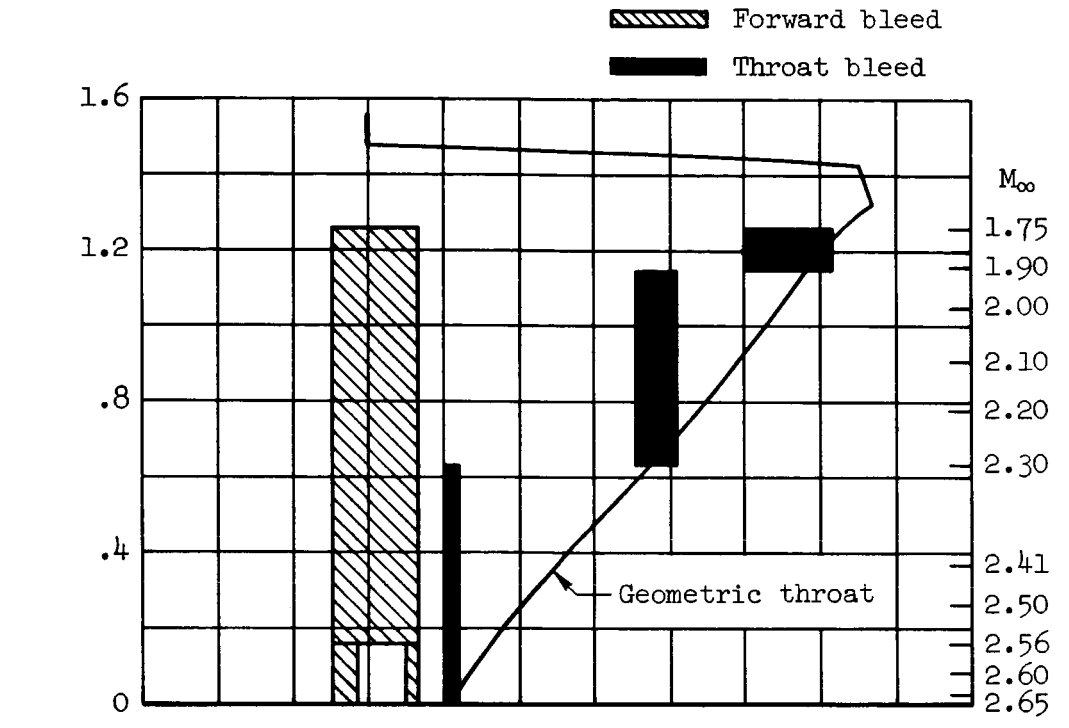

Configuration B-1 (previous inlet)

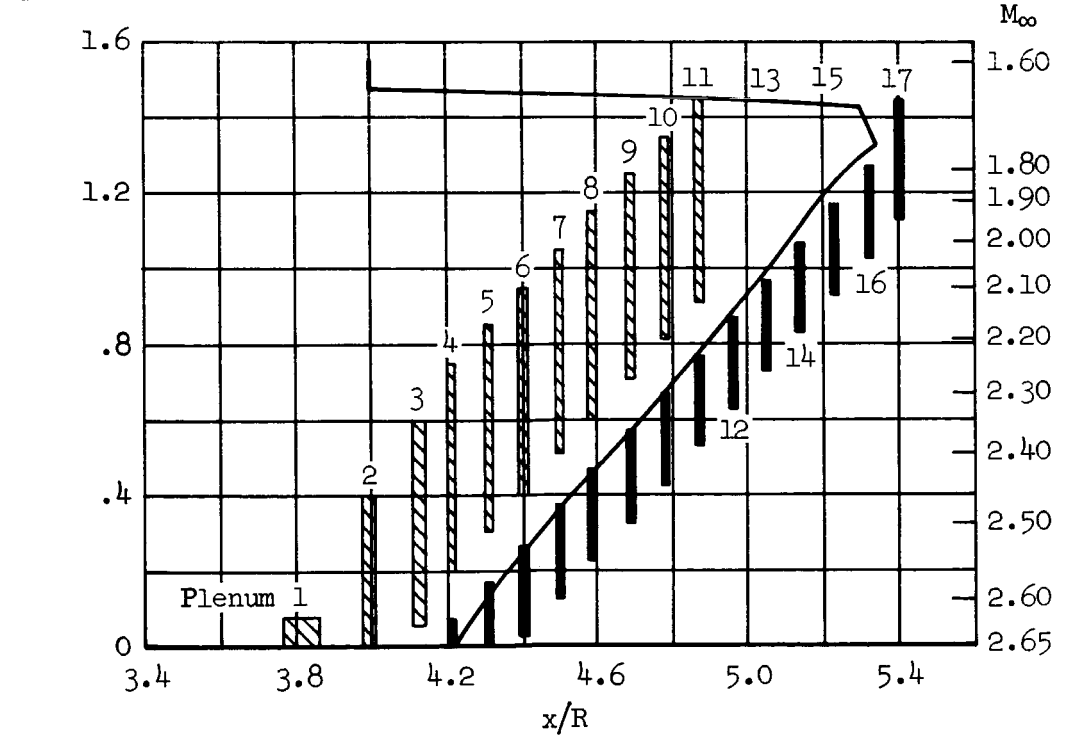

Configuration 18 (present inlet)

Figure 20.- Comparison of centerbody bleed schedules.

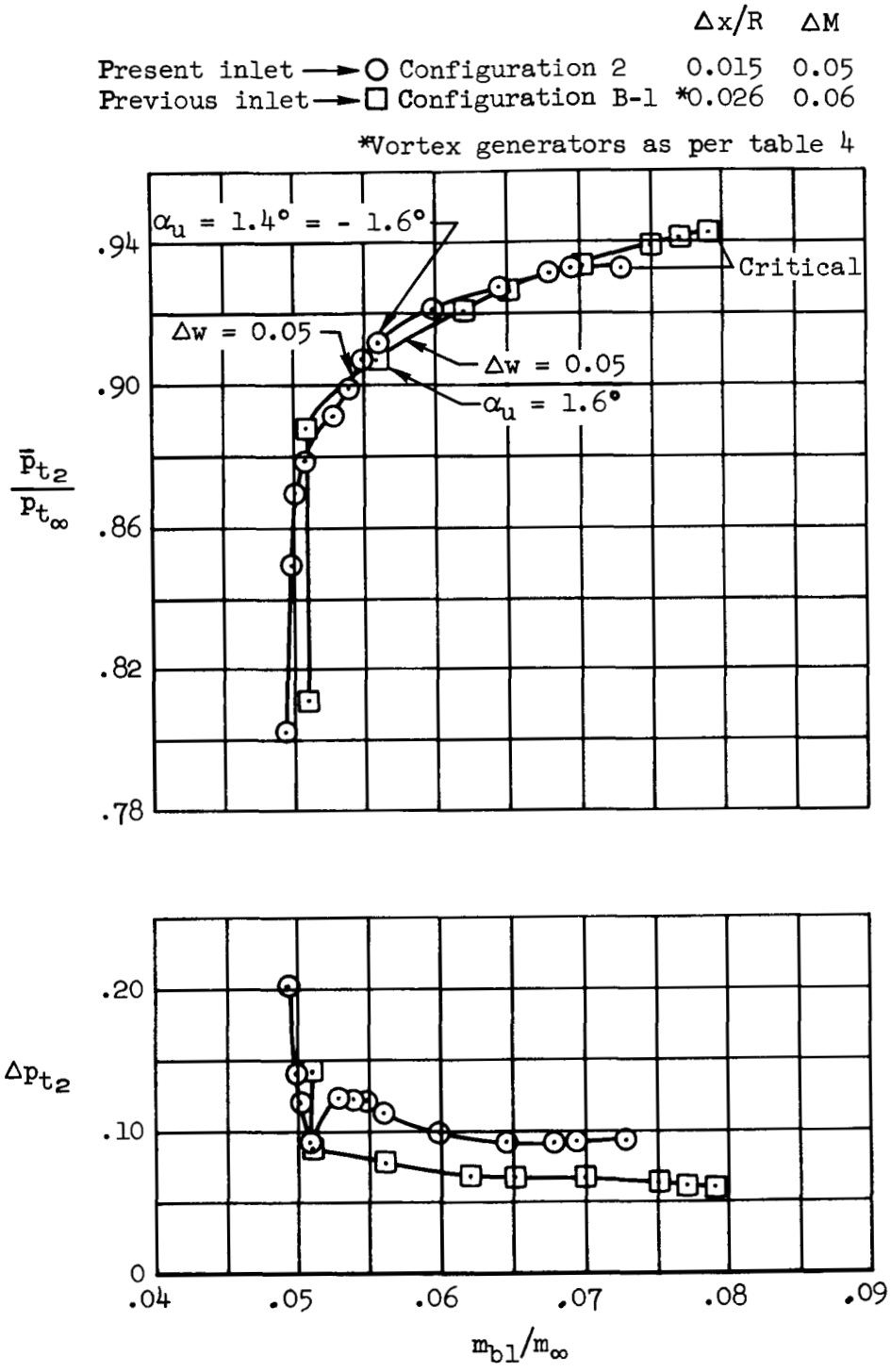

Figure 21.- Supercritical performance comparison; $M_\infty = 2.65$, $\alpha = 0°$.

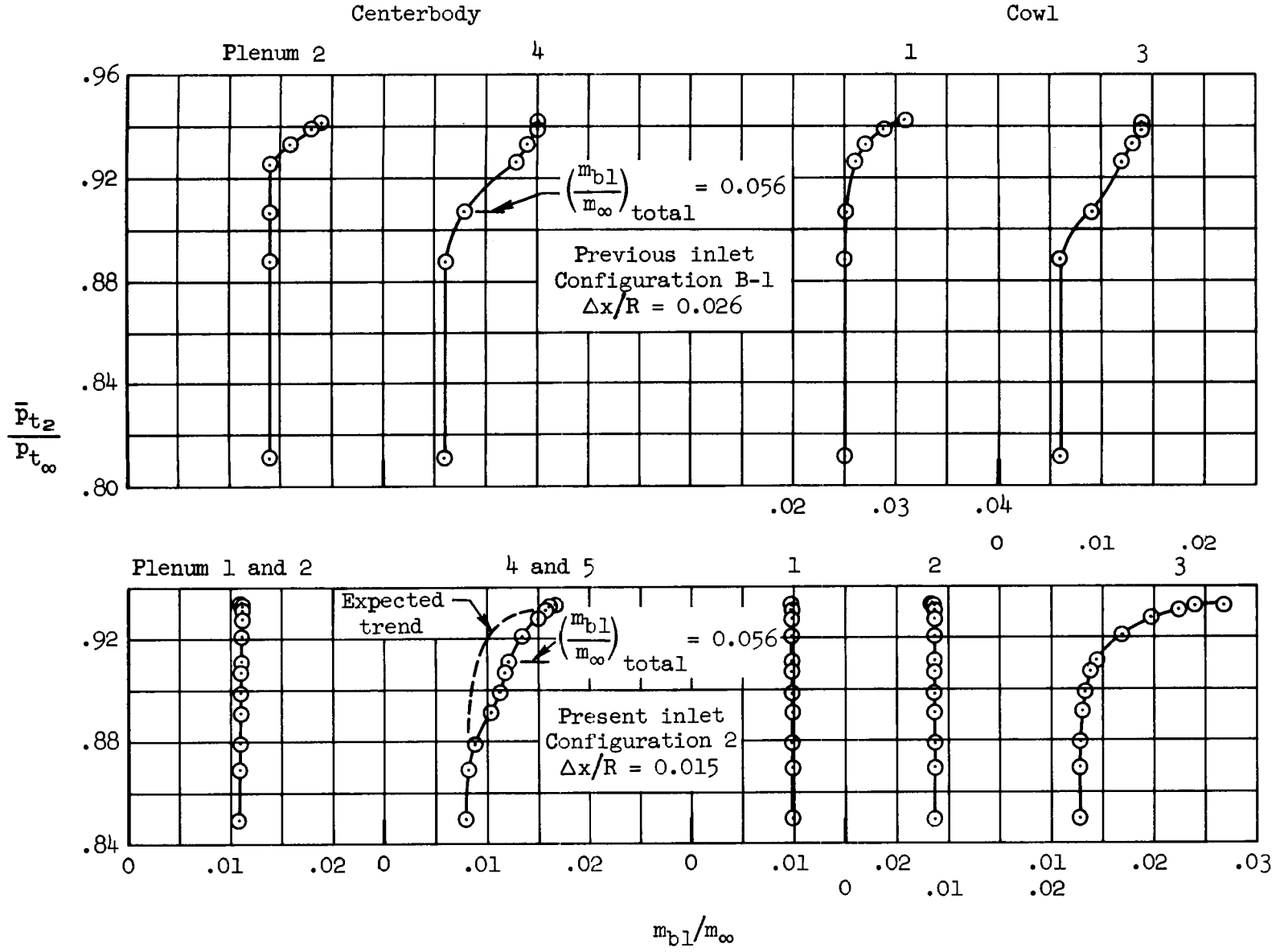

Figure 22.- Comparison of supercritical bleed flow in the individual plenums; $M_\infty = 2.65$, $\alpha = 0°$.

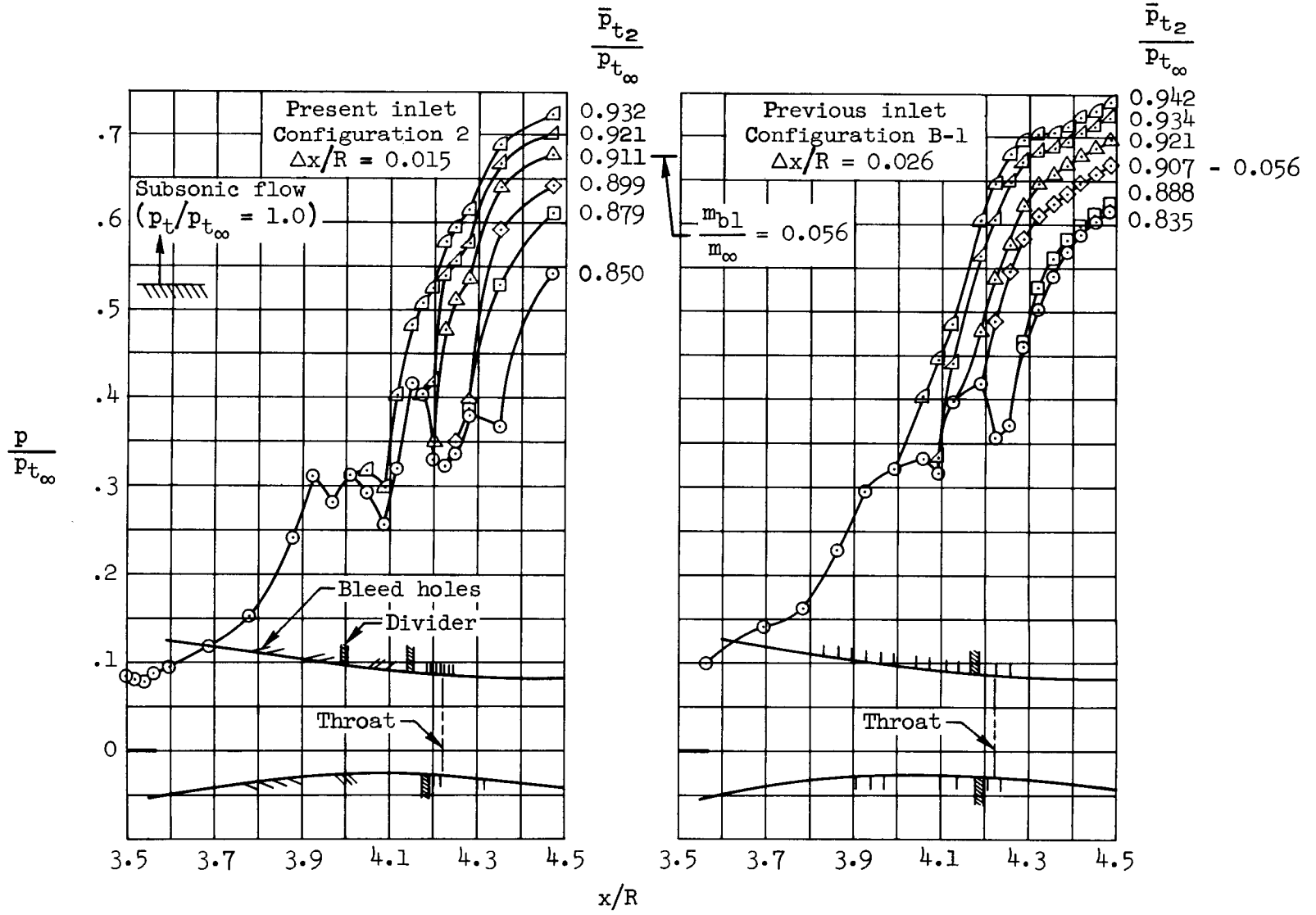

(a) Centerbody

Figure 23.- Comparison of static pressure distributions; $M_\infty = 2.65$, $\alpha = 0°$.

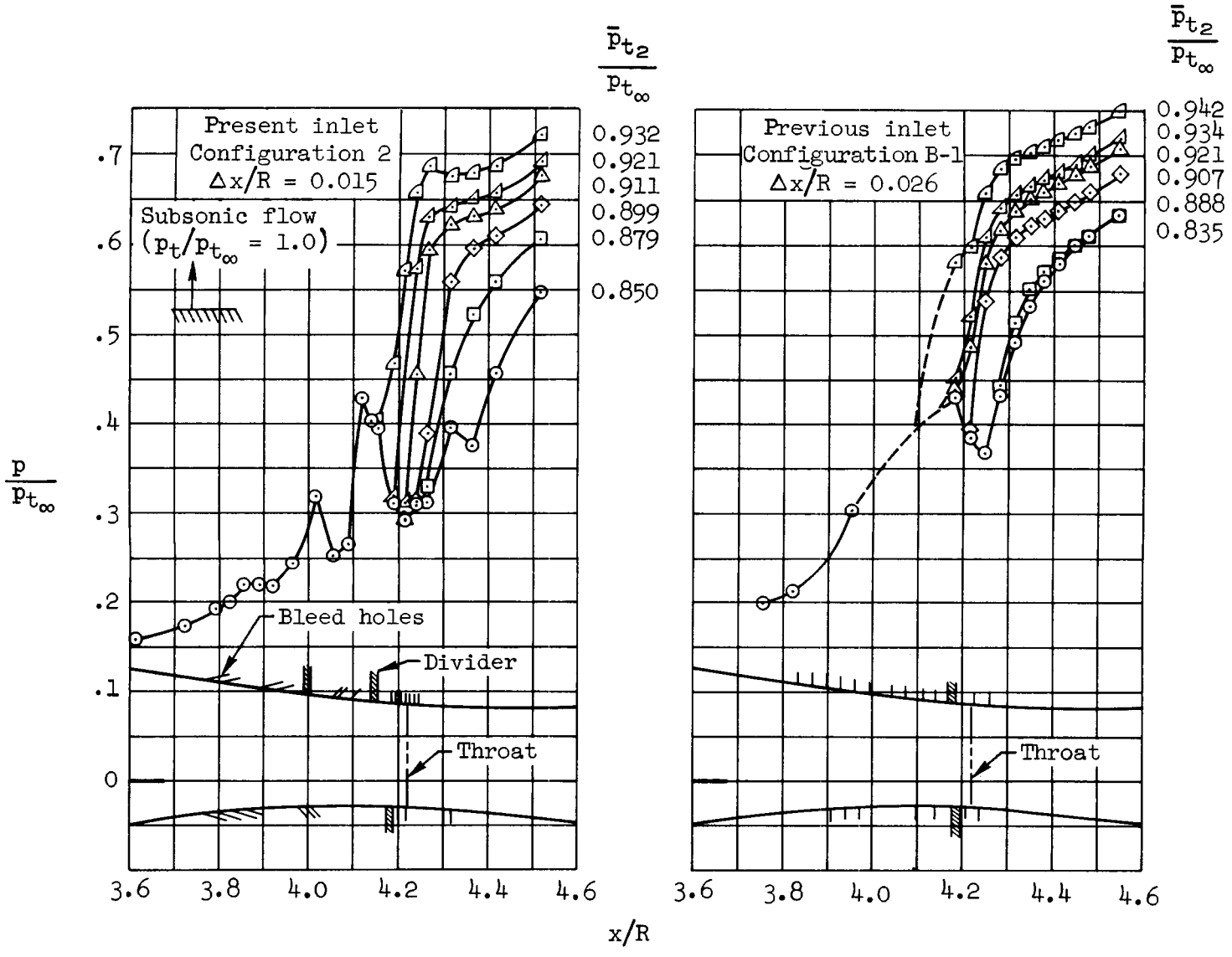

(b) Cowl

Figure 23.- Concluded.

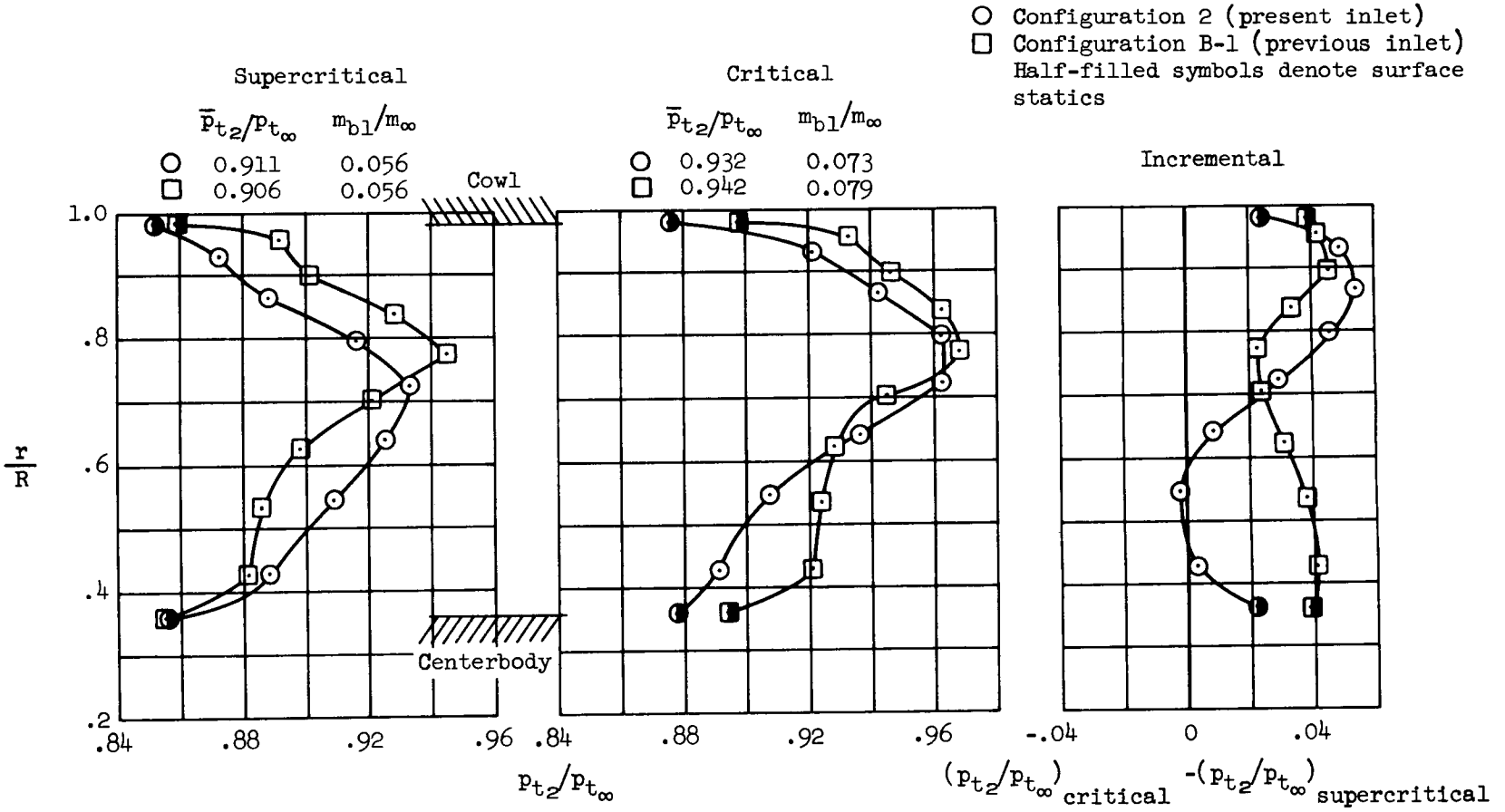

Figure 24.- Comparison of radial total-pressure profiles at the engine face; $M_\infty = 2.65$, $\alpha = 0°$.

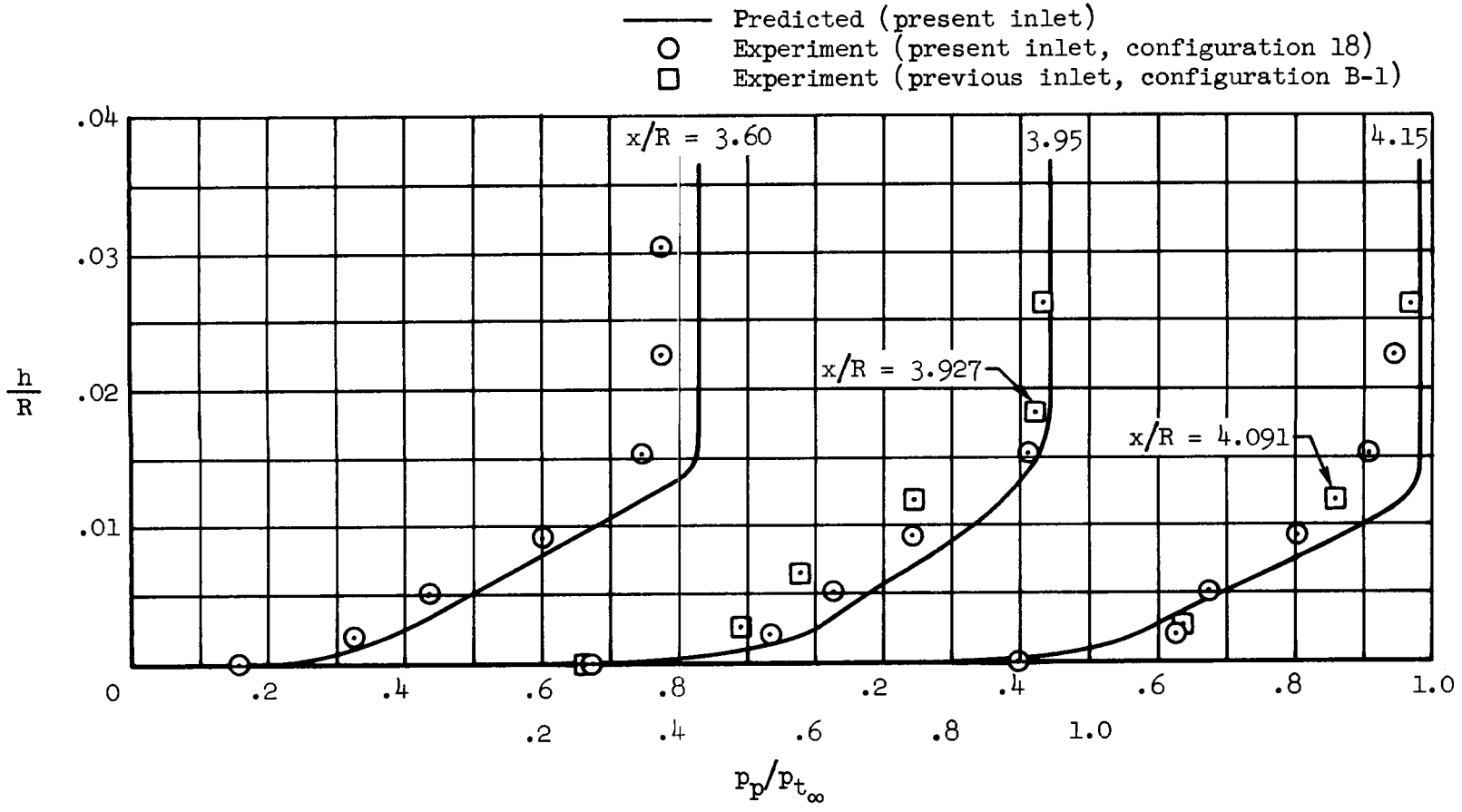

Figure 25.- Predicted and experimental cowl pitot-pressure profiles; $M_\infty = 2.65$, $\alpha = 0°$, $\Delta x/R = 0$.

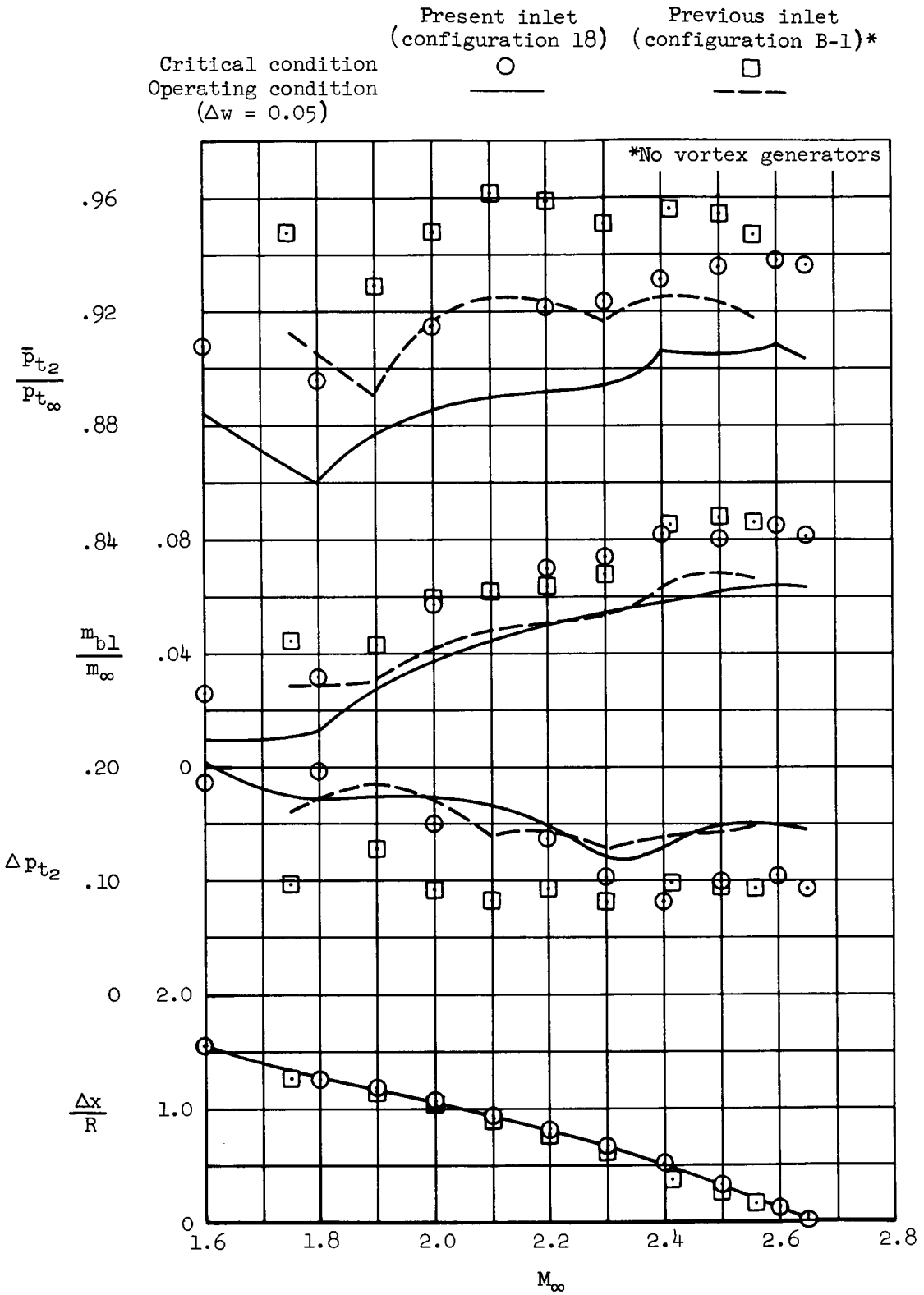

Figure 26.- Performance comparison at off-design supersonic Mach numbers; $\alpha = 0°$.

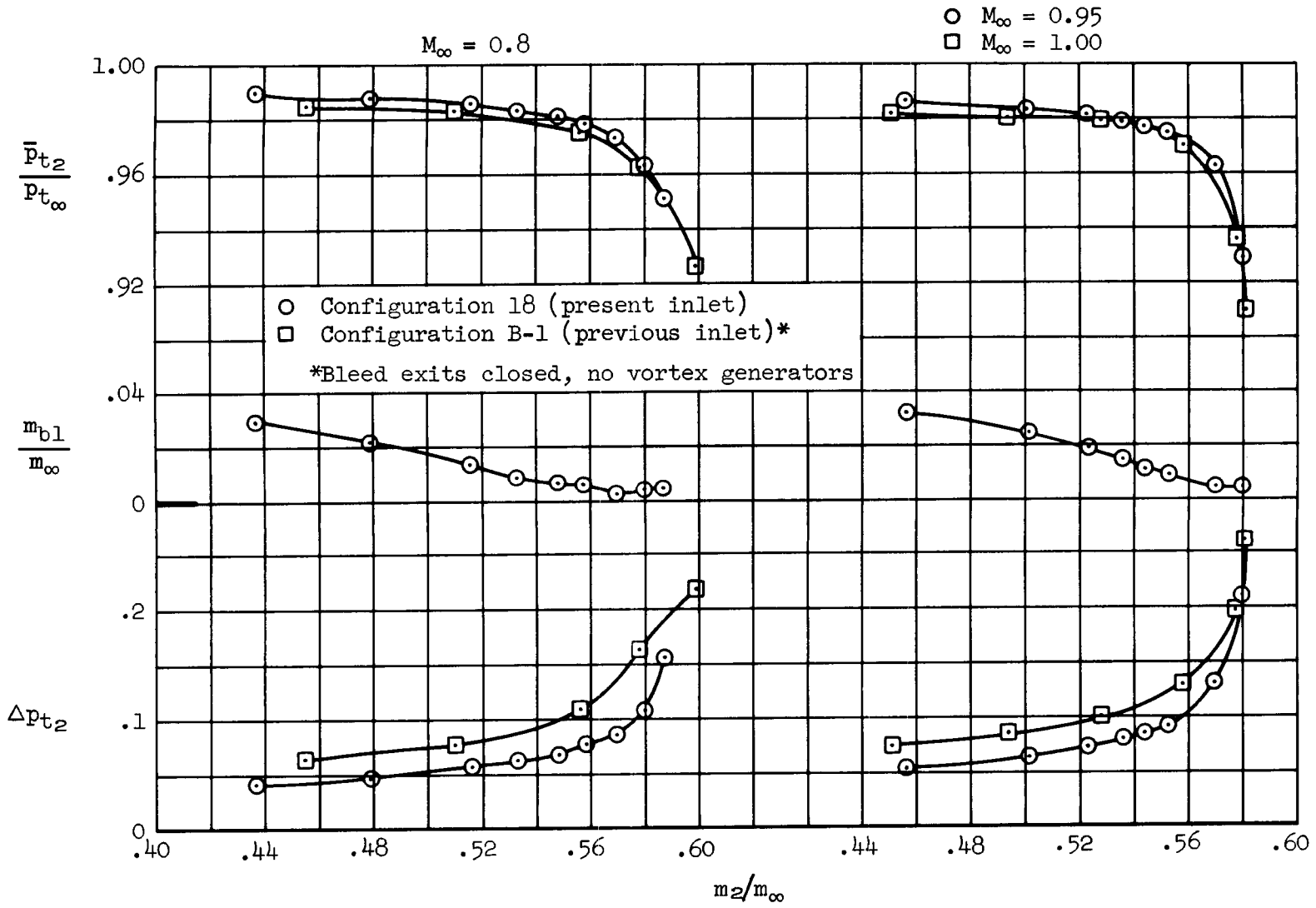

(a) $M_\infty = 0.8 \rightarrow 1.0$

Figure 27.- Comparison of transonic performance; $\alpha = 0°$, $\Delta x/R = 1.555$.

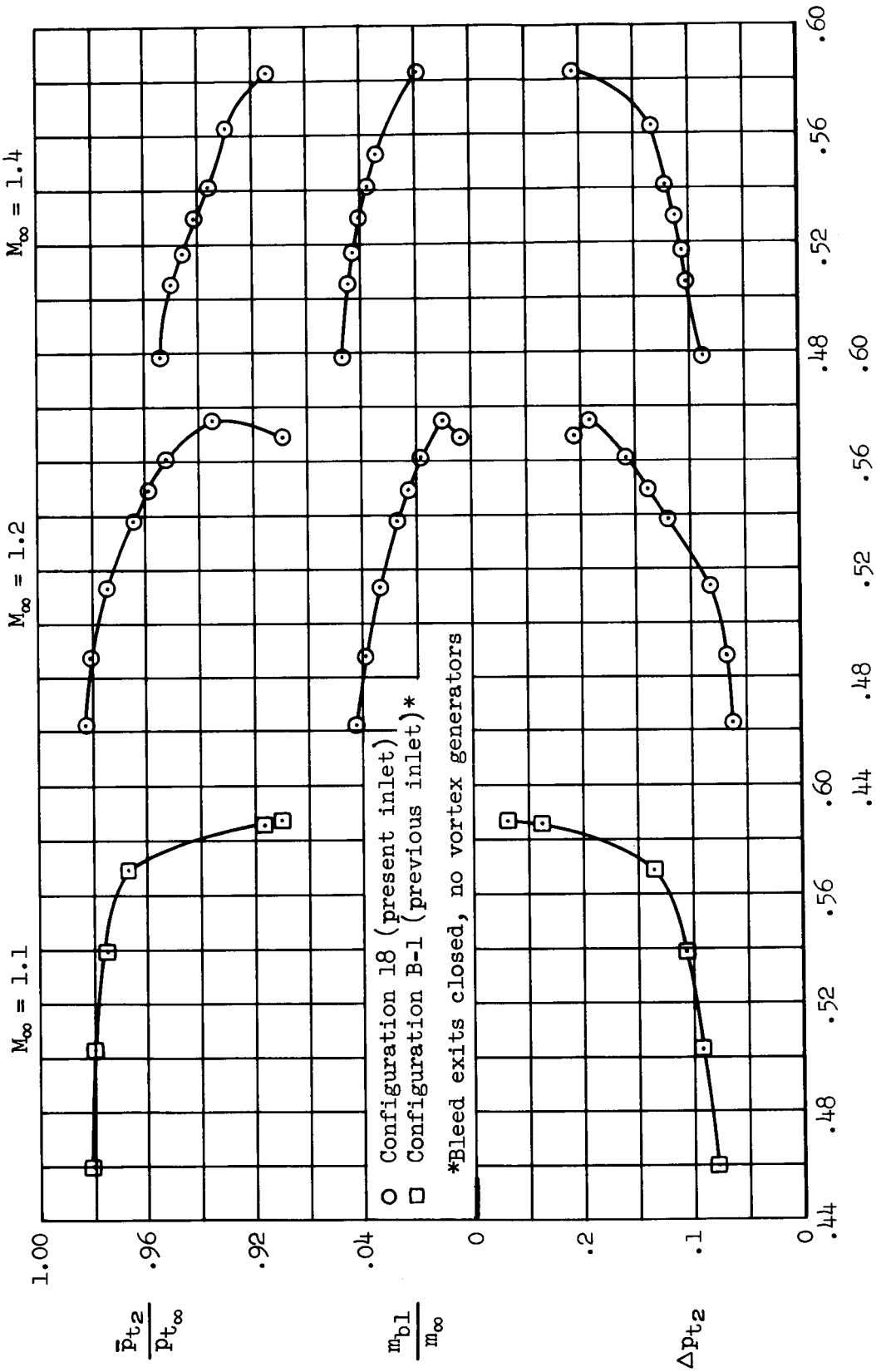

(b) M_∞ = 1.1 → 1.4

Figure 27.- Concluded.

NASA-Langley, 1973 —— 28 A-4675